

# ON THE COMPUTATIONAL COMPLEXITY OF GEOMETRIC LANGEVIN MONTE CARLO

BY THEODORE PAPAMARKOU<sup>\*</sup>, ERIC B. FORD<sup>†</sup> AND ALEXEY LINDO<sup>\*</sup>

*University of Glasgow<sup>\*</sup> and The Pennsylvania State University<sup>†</sup>*

Manifold Markov chain Monte Carlo algorithms have been introduced to sample more effectively from challenging target densities exhibiting multiple modes or strong correlations. Such algorithms exploit the local geometry of the parameter space, thus enabling chains to achieve a faster convergence rate when measured in number of steps. However, often acquiring local geometric information increases computational complexity per step to the extent that sampling from high-dimensional targets becomes inefficient in terms of total computational time. This paper analyzes the computational complexity of manifold Langevin Monte Carlo and proposes a manifold adaptive Monte Carlo sampler aimed at balancing the benefits of exploiting local geometry with computational requirements to achieve a high effective sample size for a given computational cost. The suggested strategy randomly switches between a local geometric and an adaptive proposal kernel via a schedule to regulate the frequency of manifold-based updates. An exponentially decaying schedule is put forward that enables more frequent updates of geometric information in early transient phases of the chain, while saving computational time in late stationary phases. The average complexity can be manually set depending on the need for geometric exploitation posed by the underlying model.

**1. Introduction.** The birth of geometric-based Markov chain Monte Carlo (MCMC) dates back to the landmark paper of [13], which introduced Hamiltonian Monte Carlo (HMC) to unite MCMC with molecular dynamics. [13] applied HMC in lattice field theory simulations of quantum chromodynamics. Statistical applications of HMC began with its use in neural network models by [44].

In the meanwhile, the Metropolis-adjusted Langevin algorithm (MALA) was proposed by [53] to harness Langevin dynamics for proposing new states in MCMC simulations. Both HMC and MALA evaluate the gradient of the target density, so they utilize local geometric flow.

The seminal work of [19] raised awareness of the differential geometric

---

*MSC 2010 subject classifications:* Primary 62F15; secondary 60J20.

*Keywords and phrases:* Bayesian inference, Markov chain Monte Carlo (MCMC), Langevin Monte Carlo, geometric Monte Carlo, adaptive Monte Carlo, astronomy.

foundations of MCMC. Given a vector of parameters  $\boldsymbol{\theta} \in \mathbb{R}^{n_\theta}$ , [19] defines a distance between two probability densities  $p(\boldsymbol{\theta})$  and  $p(\boldsymbol{\theta} + \delta\boldsymbol{\theta})$  as the quadratic form  $\delta\boldsymbol{\theta}^T G(\boldsymbol{\theta}) \delta\boldsymbol{\theta}$  for an arbitrary metric  $G(\boldsymbol{\theta})$ . Thus, the position-specific metric  $G(\boldsymbol{\theta})$  induces a Riemann manifold in the space of parameterized probability density functions  $\{p(\boldsymbol{\theta}) : \boldsymbol{\theta}\}$ . In the context of MCMC,  $G(\boldsymbol{\theta})$  depends on the current state  $\boldsymbol{\theta}$  of the simulated Markov chain. [19] uses  $G(\boldsymbol{\theta})$  to define transition kernels that explore the parameter space  $\{\boldsymbol{\theta} : \boldsymbol{\theta} \in \mathbb{R}^{n_\theta}\}$  effectively, thereby introducing Riemann manifold Langevin and Hamiltonian Monte Carlo methods.

The differential geometric basis of MCMC has been further researched since the appearance of [19]. For instance, [6] developed proposal mechanisms by following geodesic flows over the embedded manifolds of support for the target distribution. [35] replaced the auxiliary momentum variable appearing in Riemann manifold Hamiltonian Monte Carlo (RMHMC) by velocity to develop a Markov chain Monte Carlo algorithm using Lagrangian dynamics. [36] defined the so-called wormhole metric, for which distance between modes is shortened, in order to facilitate transitions between modes of multimodal target densities.

Computing the geometric entities of differential geometric MCMC methods creates a performance bottleneck that restricts the applicability of the involved methods. For example, manifold MCMC methods require to calculate the metric tensor  $G(\boldsymbol{\theta})$  of choice. Typically,  $G(\boldsymbol{\theta})$  is set to be the observed Fisher information matrix, which equals the negative Hessian of the log-target density at a specific point  $\boldsymbol{\theta}$ . Consequently, the complexity of manifold MCMC algorithms is dominated by Hessian-related computations, either the computation of gradient and Hessian or the inversion of the Hessian.

[19] introduced the simplified manifold Metropolis-adjusted Langevin algorithm (SMMALA) that is of the same order but often faster than MMALA and RMHMC in lower-dimensional parameter spaces. The faster speed of SMMALA over MMALA and RMHMC is explained by lower order terms and constant factors appearing in big-oh notation, which are ordinarily omitted but affect runtime in the case of smaller  $n_\theta$ . For this reason, SMMALA has been employed in conjunction with population MCMC for the Bayesian analysis of mechanistic models based on systems of non-linear differential equations, see [8] and [57]. Despite the capacity of SMMALA to exploit local geometric information so as to cope with non-linear correlations and modest increase in the dimensionality of the parameter space, in other cases its computational complexity can render performance inferior to other algorithms such as the Metropolis-adjusted Langevin algorithm (MALA) or

adaptive MCMC, see [7].

Various attempts have been made to ameliorate the computational implications of geometric MCMC methods. Along these lines, [37] used Gaussian processes to emulate the Hessian matrix and Christoffel symbols associated with the observed Fisher information  $G(\boldsymbol{\theta})$ . [59] developed a stochastic quasi-Newton Langevin Monte Carlo algorithm which takes into account the local geometry, while approximating the inverse Hessian by using a limited history of samples and their gradients. Alternatively, [49] used convex analysis and proximal techniques instead of differential calculus in order to construct a Langevin Monte Carlo method for high-dimensional target distributions that are log-concave and possibly not continuously differentiable.

This paper serves two purposes. Initially, it studies the computational complexity of geometric Langevin Monte Carlo algorithms. Subsequently, it develops a geometric adaptive Langevin Monte Carlo sampler that improves on the sampling efficacy of SMMALA. The proposed sampler combines a local geometric transition kernel that acquires a high effective sample size with an adaptive Metropolis transition kernel that attains a smaller computational cost than SMMALA. Moreover, the suggested algorithm performs exact metric evaluations whenever these occur, avoiding emulation or other approximations of the Hessian of the log-target density.

**2. Background.** The role of this section is to provide a brief overview of Langevin Monte Carlo and of adaptive Metropolis, which will be combined in later sections to construct the MCMC method contributed by this paper.

2.1. *Basics of Langevin Monte Carlo.* From a statistical perspective, Langevin Monte Carlo is a special case of Metropolis-Hastings with a normal proposal distribution

$$(2.1) \quad q(\boldsymbol{\theta}^*|\boldsymbol{\theta}) = \mathcal{N}(\boldsymbol{\theta}^*|\boldsymbol{\mu}(\boldsymbol{\theta}, G, \epsilon), \Sigma(G, \epsilon)),$$

where  $\boldsymbol{\theta}^*$  and  $\boldsymbol{\theta}$  denote the respective proposed and current state,  $G$  is a positive definite matrix of size  $n_\theta \cdot n_\theta$  and  $\epsilon$  refers to a tuning parameter known as the integration stepsize. The location  $\boldsymbol{\mu}(\boldsymbol{\theta}, G, \epsilon)$  is a function of  $\boldsymbol{\theta}$ ,  $G$  and  $\epsilon$ , whereas the covariance  $\Sigma(G, \epsilon)$  of the proposal density depends on  $G$  and  $\epsilon$ . Both  $\boldsymbol{\mu}(\boldsymbol{\theta}, G, \epsilon)$  and  $\Sigma(G, \epsilon)$  are defined so that the proposed states admit a Langevin diffusion approximated by a first-order Euler discretization. The Metropolis-Hastings acceptance probability is set to its standard form

$$(2.2) \quad a(\boldsymbol{\theta}, \boldsymbol{\theta}^*) = \min \left\{ \frac{p(\boldsymbol{\theta}^*)q(\boldsymbol{\theta}|\boldsymbol{\theta}^*)}{p(\boldsymbol{\theta})q(\boldsymbol{\theta}^*|\boldsymbol{\theta})}, 1 \right\}.$$

The integration stepsize  $\epsilon$ , also known as drift step, is associated with the first order Euler discretization and significantly affects the rate of state space exploration. If  $\epsilon$  is selected to be relatively large, many of the proposed candidates will be far from the current state, and are likely to have a low probability of acceptance, so the generated chain will have low acceptance rate. Reducing  $\epsilon$  will increase the acceptance rate, but the chain will take longer to traverse the state space.

In a Bayesian setting, the target is a possibly unnormalized posterior distribution  $p(\boldsymbol{\theta}|\mathbf{y})$ , where  $\mathbf{y}$  denotes the available data. Replacing  $p(\boldsymbol{\theta})$  by  $p(\boldsymbol{\theta}|\mathbf{y})$  in (2.2) makes Langevin Monte Carlo applicable in Bayesian problems.

To fully specify a Langevin Monte Carlo algorithm, the location  $\boldsymbol{\mu}(\boldsymbol{\theta}, G, \epsilon)$  and covariance  $\Sigma(G, \epsilon)$  of normal proposal (2.1) need to be defined. In what follows, variations of geometric Langevin Monte Carlo methods are distinguished by their respective proposal location and covariance.

*2.2. Metropolis-adjusted Langevin algorithm.* If  $G$  is kept constant, that is if  $G$  is not a function of the current state  $\boldsymbol{\theta}$ , then the Metropolis-adjusted Langevin algorithm (MALA) arises as

$$(2.3) \quad \boldsymbol{\mu}(\boldsymbol{\theta}, G, \epsilon) = \boldsymbol{\theta} + \frac{\epsilon^2}{2} G^{-1} \nabla_{\boldsymbol{\theta}} \log p(\boldsymbol{\theta}),$$

$$(2.4) \quad \Sigma(G, \epsilon) = \epsilon^2 G^{-1}.$$

$G$  is known as the precondition matrix, see [54]. It is typically set to be the identity matrix  $G = I$ , in which case MALA is defined in its conventional form.

MALA uses the gradient flow  $\nabla_{\boldsymbol{\theta}} \log p(\boldsymbol{\theta})$  to make proposals effectively. According to the theoretical analysis of [53], the optimal scaling  $\epsilon$  has been found to be the value of  $\epsilon$  which yields a limiting acceptance rate of 57.4% in high-dimensional parametric spaces (as  $n_{\boldsymbol{\theta}} \rightarrow \infty$ ).

*2.3. Manifold Langevin Monte Carlo.* It is possible to incorporate further geometric structure in the form of a position-dependent metric  $G(\boldsymbol{\theta})$ , as explained by [19, 63]. The Langevin diffusion is defined on a Riemann manifold endowed by the metric  $G(\boldsymbol{\theta})$ . The resulting manifold Metropolis-adjusted Langevin algorithm (MMALA) draws candidate states from a normal proposal with location and covariance given by

$$(2.5) \quad \boldsymbol{\mu}(\boldsymbol{\theta}, G(\boldsymbol{\theta}), \epsilon) = \boldsymbol{\theta} + \frac{\epsilon^2}{2} G^{-1}(\boldsymbol{\theta}) \nabla_{\boldsymbol{\theta}} \log p(\boldsymbol{\theta}) + \epsilon^2 \boldsymbol{\gamma}(\boldsymbol{\theta}),$$

$$(2.6) \quad \Sigma(G(\boldsymbol{\theta}), \epsilon) = \epsilon^2 G^{-1}(\boldsymbol{\theta}),$$

where the  $i$ -th coordinate  $\gamma_i(\boldsymbol{\theta})$  of  $\boldsymbol{\gamma}(\boldsymbol{\theta}) \in \mathbb{R}^{n_\theta}$  is

$$(2.7) \quad \gamma_i(\boldsymbol{\theta}) = \frac{1}{2} \sum_{j=1}^{n_\theta} \frac{\partial G_{ij}^{-1}(\boldsymbol{\theta})}{\partial \theta_j} = -\frac{1}{2} \sum_{j=1}^{n_\theta} \sum_{k=1}^{n_\theta} \sum_{m=1}^{n_\theta} G_{ik}^{-1}(\boldsymbol{\theta}) \frac{\partial G_{km}(\boldsymbol{\theta})}{\partial \theta_j} G_{mj}^{-1}(\boldsymbol{\theta}).$$

$\theta_j$ ,  $G_{km}(\boldsymbol{\theta})$  and  $G_{ij}^{-1}(\boldsymbol{\theta})$  in (2.7) denote the  $j$ -th coordinate of  $\boldsymbol{\theta}$ ,  $(k, m)$ -th element of  $G(\boldsymbol{\theta})$  and  $(i, j)$ -th element of  $G^{-1}(\boldsymbol{\theta})$ , respectively.

As seen from (2.7), the term  $\boldsymbol{\gamma}(\boldsymbol{\theta})$  increases the computational complexity of the proposal for target distributions with high number  $n_\theta$  of dimensions or with high correlation between parameters. To reduce the computational cost,  $\boldsymbol{\gamma}(\boldsymbol{\theta})$  can be dropped from (2.5), simplifying the proposal location to

$$(2.8) \quad \boldsymbol{\mu}(\boldsymbol{\theta}, G(\boldsymbol{\theta}), \epsilon) = \boldsymbol{\theta} + \frac{\epsilon^2}{2} G^{-1}(\boldsymbol{\theta}) \nabla_{\boldsymbol{\theta}} \log p(\boldsymbol{\theta}).$$

The method with location and covariance specified by (2.8) and (2.6) is known as simplified Metropolis-adjusted Langevin algorithm (SMMALA).

The optimal stepsize  $\epsilon$  for MMALA and SMMALA is empirically suggested by [19] to be set so as to obtain an acceptance rate of around 70%; this choice has not been analyzed yet from a theoretical standpoint analogously to the choice of scaling for MALA by [53].

*2.4. Differences between Langevin Monte Carlo algorithms.* The proposal mechanisms of MALA, SMMALA and MMALA define valid MCMC methods that converge to the target distribution. In fact, if the metric  $G(\boldsymbol{\theta})$  is constant, then  $\boldsymbol{\gamma}(\boldsymbol{\theta})$  vanishes, hence SMMALA and MMALA coincide with pre-conditioned MALA.

Each of the three samplers incorporate different amount of local geometry in the proposal mechanism. MALA makes use only of the gradient of the log-target. SMMALA relies additionally on the position-specific metric tensor  $G(\boldsymbol{\theta})$ . MMALA takes into account the curvature of the manifold induced by  $G(\boldsymbol{\theta})$ , which implies calculating the metric derivatives  $\partial G_{km}(\boldsymbol{\theta})/\partial \theta_j$  in (2.7). Depending on the characteristics of the manifold and its curvature, the proposals of the three Langevin Monte Carlo samplers may exhibit varying efficiency in converging to the stationary distribution, thus leading to differences in effective sample size.

On the other hand, increasing inclusion of local geometry in the proposal mechanism signifies escalating computational complexity. More specifically, MALA, SMMALA and MMALA require computing first, second and third order derivatives of the target. It is thus clear that there is a trade-off between geometric exploitation of the target from within the proposal and associated complexity of the proposal, which translates to a trade-off between effective sample size and runtime for MALA, SMMALA and MMALA.

2.5. *Basics of adaptive Metropolis.* Sampling methods that propose samples by using past values of the chain, thus breaking the Markov property, are referred to as adaptive Monte Carlo. The first adaptive Metropolis (AM) algorithm, as introduced by [25], used a proposal distribution based on the empirical covariance matrix of the whole chain at each iteration.

In its first appearance in [25], the AM algorithm was defined for target distributions of bounded support to ensure convergence to the target. [52] extended AM to work with targets of unbounded support by suggesting a mixture proposal distribution also based on the empirical covariance matrix of the whole chain at each iteration.

Several variations of the AM algorithm have been proposed. For example, [24] combined adaptive Metropolis and delayed rejection methodology to construct the delayed rejection adaptive Metropolis (DRAM) sampler, which outperforms its constituent methods in certain situations. More recently, [60] introduced the so-called robust adaptive Metropolis (RAM) algorithm, which scales the empirical covariance matrix of the chain to yield a desired mean acceptance rate, typically 23.4% in multidimensional settings. A thorough overview of adaptive Metropolis methods can be found in [23].

The ergodicity properties of adaptive MCMC were studied in [2, 51]. In particular, [51] defined the diminishing adaptation and bounded convergence conditions. Their joint satisfaction is sufficient to ensure asymptotic convergence to the target distribution. Thus, diminishing adaptation and bounded convergence provide a useful machinery for constructing adaptive MCMC algorithms.

2.6. *The first adaptive Metropolis algorithm.* Let  $(\boldsymbol{\theta}_0, \boldsymbol{\theta}_1, \dots, \boldsymbol{\theta}_k)$  be a chain simulated up to iteration  $k$ , denoted by  $\boldsymbol{\theta}_{0:k}$ , with  $i$ -th state  $\boldsymbol{\theta}_i \in \mathbb{R}^{n_\theta}$ . [25] defined the proposal kernel of adaptive Metropolis (AM) for the next candidate state  $\boldsymbol{\theta}^*$  to be the normal distribution

$$(2.9) \quad q(\boldsymbol{\theta}^* | \boldsymbol{\theta}_k) = \mathcal{N}(\boldsymbol{\theta}^* | \boldsymbol{\theta}_k, \beta S(\boldsymbol{\theta}_{0:k}) + \lambda \beta I)$$

with mean equal to the current point  $\boldsymbol{\theta}_k$  and covariance  $\beta S(\boldsymbol{\theta}_{0:k}) + \lambda \beta I$  based on the empirical covariance matrix

$$(2.10) \quad S(\boldsymbol{\theta}_{0:k}) = \frac{1}{k} \left( \sum_{i=0}^k \boldsymbol{\theta}_i \boldsymbol{\theta}_i^T - (k+1) \bar{\boldsymbol{\theta}}_k \bar{\boldsymbol{\theta}}_k^T \right)$$

of the whole history  $\boldsymbol{\theta}_{0:k}$ . A small positive constant  $\lambda$  appears in (2.9) to constrain the empirical covariance within  $c_1 I \leq S(\boldsymbol{\theta}_{0:k}) \leq c_2 I$  for some constants  $c_1, c_2 > 0$ , thereby ensuring convergence for target distributions

of bounded support. A tuning parameter  $\beta$  in (2.9), which may only depend on dimension  $n_\theta$ , allows to scale the covariance of the proposal kernel.

It follows from (2.10) that the empirical covariance at the  $k$ -th AM iteration calculates recursively as

$$(2.11) \quad kS(\boldsymbol{\theta}_{0:k}) = (k-1)S(\boldsymbol{\theta}_{0:k-1}) + \boldsymbol{\theta}_k \boldsymbol{\theta}_k^T - (k+1)\bar{\boldsymbol{\theta}}_k \bar{\boldsymbol{\theta}}_k^T + k\bar{\boldsymbol{\theta}}_{k-1} \bar{\boldsymbol{\theta}}_{k-1}^T.$$

The sample mean in (2.11) is also calculable recursively according to

$$(2.12) \quad k\bar{\boldsymbol{\theta}}_k = (k-1)\bar{\boldsymbol{\theta}}_{k-1} + \boldsymbol{\theta}_k.$$

The recursive equations (2.11) and (2.12) make the empirical covariance and sample mean of the chain computationally tractable for an arbitrarily large chain length.

2.7. *Adaptive Metropolis with mixture proposal.* [52] initiated AM with proposal kernel at iteration  $k$  given by

$$(2.13) \quad q(\boldsymbol{\theta}^* | \boldsymbol{\theta}_k) = (1-\lambda)\mathcal{N}(\boldsymbol{\theta}^* | \boldsymbol{\theta}_k, \beta S(\boldsymbol{\theta}_{0:k})) + \lambda\mathcal{N}(\boldsymbol{\theta}^* | \boldsymbol{\theta}_k, \gamma I).$$

The transition kernel defined by (2.13) is a mixture distribution, where the first component is updated adaptively using the whole chain history  $\boldsymbol{\theta}_{0:k}$  in the calculation of the empirical covariance matrix  $S(\boldsymbol{\theta}_{0:k})$  and the second component is introduced to stabilize the algorithm. A small positive constant  $\lambda$  in (2.13) ensures convergence for a large family of target densities of unbounded support, including those that are log-concave outside some arbitrary bounded region. Two tuning parameters appear in (2.13), namely  $\beta$  and  $\gamma$ , which may only depend on dimension  $n_\theta$ . Each of these parameters allow to scale the covariance of the respective mixture component.

### 3. Complexity bounds for geometric Langevin Monte Carlo.

This section provides upper bounds for the computational complexity of geometric Langevin Monte Carlo. It concludes with a short overview of the computational cost of adaptive Metropolis algorithms.

3.1. *Complexity bounds for differentiation computations.* Calculations associated with the proposal and target densities determine the computational cost of Langevin Monte Carlo methods. In brief, the main computational requirements include sampling from and evaluating the proposal, as well as evaluating the target and its derivatives.

According to (2.4), the proposal covariance  $\epsilon^2 G^{-1}$  of MALA is constant, therefore it is derivative-free. By contrast, the proposal covariance  $\epsilon^2 G^{-1}(\boldsymbol{\theta})$

of SMMALA and MMALA introduced in (2.6) require to compute the negative Hessian of the log-target as the position-specific metric  $G(\boldsymbol{\theta})$ . As seen from (2.3), (2.8) and (2.5), the proposal location of MALA, SMMALA and MMALA entail the gradient, Hessian and Hessian derivatives of the log-target. Hence, fully specifying the normal proposal distribution of MALA, SMMALA and MMALA requires up to first, second and third order derivatives of the log-target.

Assume an  $n_\theta$ -dimensional log-target with complexity  $\mathcal{O}(f(n_\theta))$ , with the notation indicating dependence of  $f$  on  $n_\theta$ . Considering the highest order of log-target differentiation associated with each sampler, it follows that the incurring costs for target-related evaluations in MALA, SMMALA and MMALA grow as  $\mathcal{O}(f(n_\theta)n_\theta)$ ,  $\mathcal{O}(f(n_\theta)n_\theta^2)$  and  $\mathcal{O}(f(n_\theta)n_\theta^3)$ , respectively.

*3.2. Complexity bounds for linear algebra computations.* Given the computed log-target and its derivatives, the Langevin Monte Carlo normal proposal (2.1) is available to sample from and evaluate. The major computational cost of evaluating and sampling from the normal proposal (2.1) is related to linear algebra calculations, namely to the inversion and Cholesky decomposition of the proposal covariance  $\epsilon^2 G^{-1}(\boldsymbol{\theta})$ .

A candidate state  $\boldsymbol{\theta}^*$  can be sampled from the normal proposal distribution (2.1) of a Langevin Monte Carlo method with mean  $\boldsymbol{\mu}(\boldsymbol{\theta}, G, \epsilon)$  and covariance  $\epsilon^2 G^{-1}(\boldsymbol{\theta})$  in the Cholesky approach by letting

$$\boldsymbol{\theta}^* = \boldsymbol{\mu}(\boldsymbol{\theta}, G, \epsilon) + \epsilon \left( \sqrt{G^{-1}(\boldsymbol{\theta})} \right)' \tau,$$

where  $\sqrt{G^{-1}(\boldsymbol{\theta})}$  satisfies the Cholesky decomposition

$$\left( \sqrt{G^{-1}(\boldsymbol{\theta})} \right)' \sqrt{G^{-1}(\boldsymbol{\theta})} = G^{-1}(\boldsymbol{\theta})$$

and  $\tau \sim \mathcal{N}(\mathbf{0}, I)$ , [10]. So, sampling from the proposal has a complexity of  $\mathcal{O}(2n_\theta^3)$ , since it requires the inversion of metric  $G(\boldsymbol{\theta})$  and the Cholesky decomposition of  $G^{-1}(\boldsymbol{\theta})$ , each of which are  $\mathcal{O}(n_\theta^3)$  operations.

To calculate the Metropolis-Hastings acceptance ratio (2.2) of SMMALA and MMALA, it is required to evaluate the normal proposal at  $\boldsymbol{\theta}$ . As it has become apparent, a proposal evaluation has a complexity of  $\mathcal{O}(n_\theta^3)$  due to the inversion of  $G(\boldsymbol{\theta})$  needed by the proposal covariance  $\epsilon^2 G^{-1}(\boldsymbol{\theta})$ .

To be precise, the normal proposal kernel (2.1) must be evaluated twice, once at  $\boldsymbol{\theta}$  and once at  $\boldsymbol{\theta}^*$ , due to its appearance both in the numerator and denominator of the acceptance ratio (2.2). This implies twice the number of log-target differentiations and matrix inversions to compute  $G(\boldsymbol{\theta})$ ,  $G(\boldsymbol{\theta}^*)$

and their inverses. Nevertheless, the scaling factor of two can be omitted in big- $\mathcal{O}$  bounds since the numerics associated with the current state  $\boldsymbol{\theta}$  are known from the previous iteration, with the exception of  $\sqrt{G^{-1}(\boldsymbol{\theta})}$ .

In summary, SMMALA and MMALA require the Cholesky factorization  $\sqrt{G^{-1}(\boldsymbol{\theta})}$  to sample  $\boldsymbol{\theta}^*$  from the normal proposal  $q(\cdot|\boldsymbol{\theta})$  and the matrix inverse  $G^{-1}(\boldsymbol{\theta}^*)$  to evaluate the normal proposal  $q(\cdot|\boldsymbol{\theta}^*)$  at  $\boldsymbol{\theta}$ . Consequently, the cost of linear algebra computations associated with the transition kernel (2.1) is of order  $\mathcal{O}(2n_\theta^3)$  for each of these two samplers.

Owing to the works of [11], [61] and [38], the Coppersmith-Winograd algorithm has been optimized to perform matrix multiplication and therefore matrix inversion in  $\mathcal{O}(n_\theta^{2.373})$  time. Hence, optimized implementations of SMMALA and MMALA can evaluate and sample from their proposal kernels in  $\mathcal{O}(n_\theta^3 + n_\theta^{2.373})$  time given the log-target and its derivatives.

MALA, as opposed to SMMALA and MMALA, relies on a constant preconditioning matrix  $G$ , therefore  $G^{-1}$  and  $\sqrt{G^{-1}}$  are evaluated once and cached at the beginning of the simulation avoiding the  $\mathcal{O}(2n_\theta^3)$  penalty. Since the preconditioning matrix  $G$ , its inverse  $G^{-1}$  and the Cholesky decomposition  $\sqrt{G^{-1}}$  are cached upon initialization for MALA, the quadratic form  $(\boldsymbol{\theta}^* - \boldsymbol{\theta})'G^{-1}(\boldsymbol{\theta}^* - \boldsymbol{\theta})$  in the normal proposal density dictates a time complexity of  $\mathcal{O}(n_\theta^2)$ . If  $G$  is set to be the identity matrix, then  $(\boldsymbol{\theta}^* - \boldsymbol{\theta})'G^{-1}(\boldsymbol{\theta}^* - \boldsymbol{\theta})$  simplifies to the inner product  $\langle \boldsymbol{\theta}^* - \boldsymbol{\theta}, \boldsymbol{\theta}^* - \boldsymbol{\theta} \rangle$  and the complexity of linear algebra calculations associated with the MALA proposal further reduces to order  $\mathcal{O}(n_\theta)$ .

*3.3. Comparison of differentiation and linear algebra costs.* Adding up the differentiation and linear algebra computational cost yields the order of complexity for Langevin Monte Carlo. Hence, it follows that MALA, SMMALA and MMALA run in  $\mathcal{O}(f(n_\theta)n_\theta + n_\theta^2)$ ,  $\mathcal{O}(f(n_\theta)n_\theta^2 + n_\theta^3 + n_\theta^{2.373})$  and  $\mathcal{O}(f(n_\theta)n_\theta^3 + n_\theta^3 + n_\theta^{2.373})$  time, respectively.

For simple models, the order of complexity of the log-target is not greater than that of the proposal, so it is assumed that the log-target scales as  $\mathcal{O}(1)$ . Thus, for simple models, the respective complexity bounds for MALA, SMMALA and MMALA reduce to  $\mathcal{O}(n_\theta^2)$ ,  $\mathcal{O}(n_\theta^3)$  and  $\mathcal{O}(n_\theta^3)$  after dropping scaling factors and lower-order terms. The complexity order of the typical MALA with identity preconditioning matrix further reduces to  $\mathcal{O}(n_\theta)$  for a simple model.

On the other hand, computationally expensive models are characterized by  $\mathcal{O}(f(n_\theta)) \gg \mathcal{O}(n_\theta)$ . For such models, the cost of computations implicating the log-target is much higher than the cost of proposal-related calculations. In other words, if the log-target is of high complexity, then derivative

computations supersede linear algebra calculations, and this is why the computational cost of a manifold MCMC algorithm tends to be reported as a function of the order of derivatives appearing in the algorithm. For instance, the complexity of SMMALA, which scales as  $\mathcal{O}(f(n_\theta)n_\theta^2 + n_\theta^3 + n_\theta^{2.373})$ , can be simply written as  $\mathcal{O}(f(n_\theta)n_\theta^2)$  for a computationally intensive model.

A typical example of a computationally expensive model is a system of non-linear ordinary differential equations (ODEs), where each log-target calculation requires solving the ODE system numerically. It is then expected that the log-target and its derivative evaluations will dominate the cost of Langevin Monte Carlo simulations according to the discussed complexity bounds.

A detailed account of the time complexity of SMMALA has been given to highlight the main sources of computational load involved in geometric updates. In what follows, scaling factors and constants will be suppressed in big- $\mathcal{O}$  notation.

*3.4. Complexity bounds for adaptive Metropolis.* From this point forward, the term adaptive Metropolis (AM) will refer to the AM algorithm of [52] with mixture proposal (2.13), as interest is in targets of unbounded support. AM does not evaluate any target-related derivatives. In lieu of differentiation costs, the target-specific complexity of AM is of order  $\mathcal{O}(f(n_\theta))$ .

The mixture distribution (2.13) is centred at the current state, and the empirical covariance of the adaptive mixture component is computed recursively, therefore entailing negligible runtime costs. That is to say, fully specifying the AM proposal distribution is computationally trivial given the chain history.

Sampling from and evaluating the fully specified normal mixture (2.13) of AM incurs the typical linear algebra computational costs encountered in Langevin Monte Carlo, namely a Cholesky decomposition and an inversion of the empirical covariance matrix  $S(\boldsymbol{\theta}_{0:k})$ . So, linear algebra manipulations of the AM proposal amount to a complexity of order  $\mathcal{O}(2n_\theta^3)$ .

The recursive formula (2.11) allows to replace the Cholesky factorization of  $S(\boldsymbol{\theta}_{0:k})$  by two rank one updates and one rank one downdate, thus reducing the Cholesky runtime bound in AM from  $\mathcal{O}(n_\theta^3)$  to  $\mathcal{O}(3n_\theta^2)$ . [18] and [58] elaborate on low rank updates for Cholesky decompositions.

In total, the computational cost of AM sums up to  $\mathcal{O}(f(n_\theta) + 2n_\theta^3)$ . It reduces to  $\mathcal{O}(f(n_\theta) + n_\theta^{2.373} + 3n_\theta^2)$  if optimized algorithms are chosen to invert  $S(\boldsymbol{\theta}_{0:k})$  and low rank updates are used for factorizing  $S(\boldsymbol{\theta}_{0:k})$ .

For simple targets scaling as  $\mathcal{O}(1)$ , AM takes up to  $\mathcal{O}(2n_\theta^3)$  operations, so it is more costly than MALA and cheaper than SMMALA and MMALA.

For expensive targets with complexity  $\mathcal{O}(f(n_\theta)) \gg \mathcal{O}(n_\theta)$ , AM runs in  $\mathcal{O}(f(n_\theta))$  time, so it is cheaper than MALA, SMMALA and MMALA.

#### 4. Manifold adaptive Metropolis-adjusted Langevin algorithm.

Manifold Langevin Monte Carlo pays a higher computational price than adaptive Metropolis to achieve increased effective sample size via geometric exploitation of the target. To get the best of both worlds, the goal is to construct a Monte Carlo sampler that attains fast mixing per step but with less cost per step.

4.1. *The idea.* Along these lines, the present paper introduces a hybrid sampling method that switches between expensive geometric Langevin Monte Carlo (LMC) and cheap adaptive Metropolis (AM) updates. At iteration  $k$ , an indicator  $b_k \in \{0, 1\}$  is used for setting the suggested kernel  $q^{(k)}(\star|\cdot, b_k)$  to be either the LMC transition kernel  $q_\ell(\star|\cdot)$  or the AM transition kernel  $q_\alpha(\star|\cdot)$  according to

$$(4.1) \quad q^{(k)}(\star|\cdot, b_k) = b_k q_\ell(\star|\cdot) + (1 - b_k) q_\alpha(\star|\cdot).$$

Depending on whether  $b_k$  is acquired deterministically or stochastically, sampling a state  $\theta^*$  from  $q^{(k)}(\star|\theta_k, b_k)$  given the current state  $\theta_k$  and  $b_k$  defines a stochastic process in a varying or random environment, respectively. If  $b_k$  is realized randomly and  $\theta^*$  is subsequently drawn from  $q^{(k)}(\star|\theta_k, b_k)$ , then the process of proposing a new state  $\theta^*$  involves double stochasticity.

For instance, the two-step process

$$(4.2) \quad b_k | p_k \sim p(b_k) = \text{Bernoulli}(p_k),$$

$$(4.3) \quad \theta^* | b_k \sim q^{(k)}(\star|\theta_k, b_k) = b_k q_\ell(\star|\theta_k) + (1 - b_k) q_\alpha(\star|\theta_k)$$

is doubly stochastic. At the  $k$ -th iteration, a Bernoulli trial  $b_k$  is made with success probability  $p_k = \text{P}(b_k = 1)$  of taking an LMC step. A state  $\theta^*$  is then sampled from the faster mixing LMC proposal density  $q_\ell(\star|\theta_k)$  if the Bernoulli trial is successful at step  $k$ , or from the more cost-effective AM proposal density  $q_\alpha(\star|\theta_k)$  otherwise.

Two clarifications about the suggested kernel specification follow. Firstly, it is noted that  $q^{(k)}(\star|\theta_k, b_k)$  in (4.3) is not a mixture distribution since  $b_k \notin (0, 1)$ . If  $b_k \in (0, 1)$  were assumed instead of  $b_k \in \{0, 1\}$ , the resulting mixture would require to evaluate its LMC component at each Monte Carlo iteration and would therefore inflict computational cost as high as geometric Langevin Monte Carlo.

Secondly, it is emphasized that the two-step process (4.2)-(4.3) is not thought of as the joint distribution  $q^{(k)}(\star, b_k|\theta_k) = q^{(k)}(\star|\theta_k, b_k)p(b_k)$ . This

**Algorithm 1** MAMALA

---

```

for  $k = 1$  to  $n_m$  do
  Sample  $b_k \sim \text{Bernoulli}(p_k)$ 

  if  $b_k = 1$  then ▷ Use LMC proposal
     $q(\star|\cdot) = \mathcal{N}(\star|\boldsymbol{\mu}(\cdot, G(\cdot), \epsilon), \epsilon^2 G^{-1}(\cdot))$ 
  else if  $b_k = 0$  then ▷ Use AM proposal
    if  $b_{k-1} = 1$  then
       $q(\star|\cdot) = (1 - \lambda)\mathcal{N}(\star|\cdot, \epsilon^2 G^{-1}(\cdot)) + \lambda\mathcal{N}(\star|\cdot, \gamma I)$ 
    else if  $b_{k-1} = 0$  then
       $q(\star|\cdot) = (1 - \lambda)\mathcal{N}(\star|\cdot, \epsilon^2 S(\boldsymbol{\theta}_{0:k})) + \lambda\mathcal{N}(\star|\cdot, \gamma I)$ 
    end if
  end if

  Sample  $u \sim \mathcal{U}(0, 1)$ 

  Sample  $\boldsymbol{\theta}^* \sim q(\star|\boldsymbol{\theta}_k)$ 

   $r = \frac{p(\boldsymbol{\theta}^*)q(\boldsymbol{\theta}_k|\boldsymbol{\theta}^*)}{p(\boldsymbol{\theta}_k)q(\boldsymbol{\theta}^*|\boldsymbol{\theta}_k)}$ 

  if  $u < r$  then
     $\boldsymbol{\theta}_{k+1} = \boldsymbol{\theta}^*$ 
  else
     $\boldsymbol{\theta}_{k+1} = \boldsymbol{\theta}_k$ 
  end if
end for

```

---

would lead to the augmented parameter space  $(\boldsymbol{\theta}_k, b_k)$ . However, such augmentation is not desired because the binary indicator  $b_k$  is independent of and thus not learnt from the data, as opposed to the auxiliary momentum variable in Hamiltonian Monte Carlo for instance. Instead, the stochastic process (4.2)-(4.3) is better understood as an annealed or quenched scheme in which the probability  $p_k$  of a geometric update is the analogue of temperature.

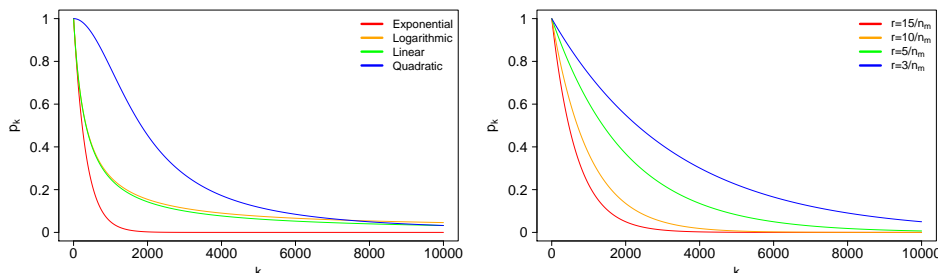
4.2. *Algorithmic formulation.* Algorithm 1 provides a pseudocode representation of the proposed Monte Carlo sampler. The sampler is called *manifold adaptive Metropolis-adjusted Langevin algorithm* (MAMALA) to highlight the duality of geometric Langevin and adaptive Metropolis updates performed by the proposal mechanism (4.1).

Algorithm 1 demonstrates that the proposal covariance is based on the position-specific metric  $G(\cdot)$  whenever possible and falls back to the empirical covariance  $S(\cdot)$  otherwise. Thus,  $G(\cdot)$  initializes  $S(\cdot)$ , and the latter is recursively updated via (2.11) until the next geometric update re-initializes

TABLE 1

Exponential, logarithmic, linear and quadratic schedules of diminishing probability  $p_k$  of geometric steps. The hyperparameters  $r$  and  $s$  tune the rate at which  $p_k$  decreases.

Type	Exponential	Logarithmic	Linear	Quadratic
$p_k$	$\exp(-r(k-1))$	$\frac{1}{1+r \log(s(k-1)+1)}$	$\frac{1}{1+r(k-1)}$	$\frac{1}{1+r(k-1)^2}$



(a) Instances of schedule types from Table 1 (b) Exponential schedule for varying  $r$

FIG 1. Schedules of diminishing probability  $p_k$  of geometric steps. (a): similarly scaled instances of Table 1; exponential, linear and quadratic schedules with  $r = 30/n_m$  and logarithmic schedule with  $r = 30$ ,  $s = 1/n_m$ , where  $n_m = 10,000$  is the total number of Monte Carlo iterations. (b): exponential schedules for different values of the tuning hyperparameter  $r$ ; as  $r$  increases, the decay rate of  $p_k$  also increases, therefore the number of geometric updates decreases almost surely.

the empirical covariance.

4.3. *Choice of schedule for geometric steps.* A design decision to make is how to set the sequence of probabilities  $\{p_k\}$  of choosing LMC over AM steps. The choice of  $\{p_k\}$  affects the ergodic properties and the computational complexity of MAMALA.

One possibility is to make the frequency of LMC steps more pronounced in early transient phases of the chain and let the computationally cheaper AM kernel take over asymptotically in late stationary phases. To this end, a monotonically decreasing sequence  $\{p_k\}$  with  $\lim_{k \rightarrow \infty} p_k = 0$  can be selected.

There is a rich literature on cooling schedules  $\{t_k\}$  for simulated annealing ([33, 26, 40, 46, 42]). Replacing the temperature  $\{t_k\}$  with  $\{p_k\}$  allows to define monotonically decreasing sequences  $\{p_k\}$  for MAMALA that cool down the probability of geometric steps to zero asymptotically. For example, Table 1 provides an exponential ([33]), logarithmic ([1]), linear and quadratic multiplicative schedule  $\{p_k\}$ . Figure 1a visualizes similarly scaled instances of the schedules of Table 1 for a total of  $n_m = 10,000$  Monte Carlo iterations

by setting  $r = 30/n_m$  for the exponential, linear and quadratic schedule, and  $r = 30$ ,  $s = 1/n_m$  for the logarithmic schedule.

Figure 1b shows four instances of the exponential schedule

$$(4.4) \quad p_k = \exp(-r(k-1)),$$

each corresponding to a different value of the tuning parameter  $r$ . Larger values of  $r$  in (4.4) yield faster reduction in the probability of using the LMC kernel.

Alternative schedules for the probability  $p_k$  of taking geometric steps can be considered. A possibility to explore would be to make an LMC proposal every  $\text{mod}(r)$  steps for some tuning parameter  $r$  or to choose randomly via a  $\text{Geometric}(r)$  distribution how many steps will be taken before the next LMC proposal is made. Both the  $\text{mod}(r)$  and  $\text{Geometric}(r)$  schedules generate a non-decreasing and asymptotically non-vanishing probability sequence  $\{p_k\}$ , hence they violate diminishing adaptation. The exploration of MAMALA under schedules that do not satisfy diminishing adaptation is deferred to the future due to challenges associated with the study of convergence of the resulting sampling strategy.

MAMALA is equipped with the exponential schedule (4.4) in this paper. Under schedule (4.4), MAMALA and AM share similar ergodic properties and complexity bounds asymptotically. Yet MAMALA has faster mixing per step than AM due to exploitation of local geometric information in early phases of the chain. The tuning parameter  $r$  in (4.4) regulates the frequency of geometric steps and therefore the ratio of mixing per step and computational cost per step.

4.4. *Convergence.* This section establishes the convergence of MAMALA under the exponential schedule (4.4).

PROPOSITION 4.1. *The ergodicity of MAMALA under the exponential schedule (4.4) for the probabilities of geometric steps is solely determined by the ergodicity of the AM transition kernel used in MAMALA.*

PROOF. Under the exponential schedule (4.4), the sum of probabilities of geometric steps over the first  $n_m$  MAMALA iterations equals

$$(4.5) \quad \sum_{k=1}^{n_m} p_k = \frac{1 - \exp(-rn_m)}{1 - \exp(-r)}.$$

It follows from (4.5) that the sum of probabilities  $\{p_k : k \in \mathbb{N}\}$  is finite,

$$\sum_{k=1}^{\infty} p_k = \lim_{n_m \rightarrow \infty} \sum_{k=1}^{n_m} p_k = \frac{1}{1 - \exp(-r)} < \infty.$$

By application of the Borel-Cantelli lemma, the LMC transition kernel  $q_\ell(\star|\cdot)$  is used only a finite number of times almost surely. Hence, if the AM transition kernel  $q_\alpha(\star|\cdot)$  is ergodic, then MAMALA is also ergodic.  $\square$

It was shown in [51] that the AM algorithm converges under the so-called diminishing adaptation and bounded convergence conditions. As noted in [52], the AM kernel (2.13) satisfies the diminishing adaptation condition. The bounded convergence condition requires the convergence time of AM to remain bounded in probability and is a lot harder to establish. Under some additional assumptions on the target distribution, the ergodicity of AM in the case of unbounded domains was obtained in [52, 56, 3].

*4.5. Expected complexity.* The concept of complexity carries three distinct meanings in the context of MCMC. Firstly, MCMC samplers need to be tuned so as to achieve a balance between proposing large enough jumps and ensuring that a reasonable proportion of jumps are accepted. By way of illustration, MALA attains its optimal acceptance rate of 57.4% as  $n_\theta \rightarrow \infty$  by setting its drift step  $\epsilon$  to be in the vicinity of  $n_\theta^{-1/3}$ . Because of this, it is said that the algorithmic efficiency of MALA scales  $\mathcal{O}(n_\theta^{1/3})$  as the number  $n_\theta$  of parameters increases.

Secondly, the quality of MCMC methods depends on their rate of mixing per step. Along these lines, the effective sample size (ESS) is used for quantifying the mixing properties of an MCMC method. The ESS of a chain of length  $n_m$  is interpreted as the number of samples in the chain bearing the same amount of variance as the one found in  $n_m$  independent samples.

A third criterion for assessing MCMC algorithms is their computational cost per step. This criterion corresponds to the ordinary concept of algorithmic complexity as it entails a count of numerical operations performed by an MCMC algorithm. To give an example, the computational complexity of MALA with an identity preconditioning matrix for a simple model is of order  $\mathcal{O}(n_\theta)$ , as explained in section 3.3.

Of these three indicators of complexity, ESS and computational runtime are the ones typically used for understanding the range of applicability of MCMC methods. To get a single-number summary, the ratio of ESS over runtime is usually employed.

The present section states the algorithmic complexity of MAMALA theoretically, while section 5 provides an empirical assessment of MAMALA via its ESS and CPU runtime.

**PROPOSITION 4.2.** *Let MAMALA conduct a Bernoulli trial  $b_k$  at iteration  $k$  with probabilities  $p_k$  and  $1 - p_k$  of choosing between its constituent*

*LMC and AM transition kernels.* Denote by  $c_\ell$  and  $c_\alpha$  the computational complexities corresponding to the LMC and AM proposal mechanisms. The expected complexity of MAMALA over the first  $n_m$  iterations is given by

$$(4.6) \quad \mathcal{O} \left( \frac{\sum_{k=1}^{n_m} p_k}{n_m} c_\ell + \frac{n_m - \sum_{k=1}^{n_m} p_k}{n_m} c_\alpha \right).$$

PROOF. The expected number of invocations of the LMC kernel equals

$$E \left( \sum_{k=1}^{n_m} b_k \right) = \sum_{k=1}^{n_m} E(b_k) = \sum_{k=1}^{n_m} p_k,$$

whence the conclusion follows directly.  $\square$

COROLLARY 4.1. *If the exponentially decaying schedule (4.4) is used for regulating the choice of transition kernel, then the expected complexity of MAMALA over the first  $n_m$  iterations expresses as*

$$(4.7) \quad \mathcal{O} \left( \frac{1 - \exp(-rn_m)}{n_m(1 - \exp(-r))} c_\ell + \left( 1 - \frac{1 - \exp(-rn_m)}{n_m(1 - \exp(-r))} \right) c_\alpha \right).$$

PROOF. Plugging (4.5) into (4.6) gives (4.7).  $\square$

COROLLARY 4.2. *For large number  $n_m$  of iterations ( $n_m \rightarrow \infty$ ), the expected complexity of MAMALA under the exponentially decaying schedule (4.4) reduces to the complexity of its AM counterpart.*

PROOF. It suffices to notice that

$$(4.8) \quad \lim_{n_m \rightarrow \infty} \frac{1 - \exp(-rn_m)}{n_m(1 - \exp(-r))} = 0.$$

Due to (4.8), the bound (4.7) diminishes asymptotically to  $\mathcal{O}(c_\alpha)$ .  $\square$

As an example, consider MAMALA equipped with the SMMALA and mixture AM kernel (2.13). In this case,  $c_\ell = \mathcal{O}(f(n_\theta)n_\theta^2)$  and  $c_\alpha = \mathcal{O}(f(n_\theta))$  for expensive targets with complexity  $\mathcal{O}(f(n_\theta)) \gg \mathcal{O}(n_\theta)$ . So, (4.7) yields an expected complexity of

$$(4.9) \quad \mathcal{O} \left( \frac{1 - \exp(-rn_m)}{n_m(1 - \exp(-r))} f(n_\theta)n_\theta^2 + \left( 1 - \frac{1 - \exp(-rn_m)}{n_m(1 - \exp(-r))} \right) f(n_\theta) \right)$$

for MAMALA, which is bounded below by the AM complexity of  $\mathcal{O}(f(n_\theta))$  and above by the SMMALA complexity of  $\mathcal{O}(f(n_\theta)n_\theta^2)$ . For instance, choosing  $n_m = 10^5$  and  $r = 10/n_m = 10^{-4}$  in (4.9) yields an expected MAMALA complexity approximately equal to  $\mathcal{O}(0.1f(n_\theta)n_\theta^2 + 0.9f(n_\theta))$ .

It follows from Corollary 4.2 that for large number  $n_m$  of iterations, the expected complexity of MAMALA in (4.9) tends to the lower bound  $\mathcal{O}(f(n_\theta))$  of AM complexity. More generally, the convergence and computational complexity of MAMALA are determined asymptotically by the AM kernel used in MAMALA, as seen from Proposition 4.1 and Corollary 4.2.

Yet the SMMALA steps in early transient phases of MAMALA provide an improvement in mixing over AM. For example, setting  $n_m = 10^5$  and  $r = 10^{-4}$  in (4.9) produces an expected 10% of SMMALA steps, which is a potentially sufficient perturbation in early stages of parameter space exploration so as to move to target modes of higher probability mass.

4.6. *Analytically intractable geometric steps.* In practice, challenges in the implementation of manifold MCMC algorithms might raise additional computational implications. In particular, two notoriously recurring issues relate to the Cholesky decomposition of metric  $G^{-1}(\boldsymbol{\theta})$  and to the calculation of up to third order derivatives of  $G(\boldsymbol{\theta})$ .

Various contributing factors, including finite-precision floating point arithmetic, can lead to an indefinite proposal covariance matrix  $\epsilon^2 G^{-1}(\boldsymbol{\theta})$ . This in turn breaks the Cholesky factorization of  $\epsilon^2 G^{-1}(\boldsymbol{\theta})$ . Several research avenues have introduced alternative positive definite approximations of indefinite matrices ([27, 28, 29]) and approximate Riemann manifold metric choices ([4, 30, 34]), which offer proxies for an indefinite proposal covariance  $\epsilon^2 G^{-1}(\boldsymbol{\theta})$ .

Non-trivial models can render the analytic derivation of log-target derivatives impossible or impractical. Automatic differentiation (AD), a computationally driven research activity that has evolved since the mid 1950's, helps compute derivatives in a numerically exact way. Indeed, [21] has shown that AD is backward stable in the sense of [62]. Thus, small perturbations of the original function due to machine precision still yield accurate derivatives calculated via AD.

There are different methods of automatic differentiation that mainly differ in the way they traverse the chain rule; reverse mode AD is better suited for functions  $f : \mathbb{R}^n \rightarrow \mathbb{R}$ , in contrast to forward mode AD that is more suitable for functions  $f : \mathbb{R} \rightarrow \mathbb{R}^m$  ([22]). Consequently, reverse mode AD is utilized for computing derivatives of probability distributions, and finds use in statistical inference. Reverse mode AD is not worse than that of the respective analytical derivatives of a target density in terms of complexity, but it poses high memory requirements. Hybrid AD procedures combining elements of forward and backward propagation of derivatives can be constructed for achieving a compromise between execution time and memory

usage when differentiating functions of the form  $f : \mathbb{R}^n \rightarrow \mathbb{R}^m$ .

**5. Simulation study.** MAMALA is compared empirically with AM, MALA and SMMALA in terms of mixing and cost per step via four examples. The examples revolve around Bayesian logistic regression, a multivariate t-distribution with correlated coordinates, and two planetary systems, one with a single planet and one with two planets.

Ten chains are generated by each sampler for each example. 110,000 iterations are run for the realization of each chain, of which the first 10,000 are discarded as burn-in, so  $n_m = 100,000$  samples per chain are retained in subsequent descriptive statistics.

To assess the quality of mixing of a sampler, the ESS of each chain generated by the sampler is computed. The ESS of each coordinate  $\theta_i$ , of the parameter vector  $\boldsymbol{\theta} \in \mathbb{R}^{n_\theta}$  is defined as

$$\text{ESS}(n_m) = \frac{n_m \hat{\sigma}_{\text{IID}}^2}{\hat{\sigma}_{\text{MC}}^2},$$

where  $\hat{\sigma}_{\text{IID}}^2$  and  $\hat{\sigma}_{\text{MC}}^2$  denote the estimated ordinary and Monte Carlo variance of the associated chain. The initial monotone sequence estimator of [17] is used for calculating  $\hat{\sigma}_{\text{MC}}^2$ .

To assess the computational cost of a sampler, the CPU runtime of each chain generated by the sampler is recorded. The ESS per parameter coordinate and CPU runtime are reported by taking their respective means across the set of ten simulated chains.

The computational efficiency of a sampler is defined as the ratio of minimum ESS among all  $n_\theta$  parameter coordinates over CPU runtime. Finally, the speed-up of a sampler relatively to MALA is set to be the ratio of MALA efficiency over the efficiency of the sampler.

A single MAMALA setup is used across all four examples. More specifically, the SMMALA kernel and mixture AM kernel (2.13) are chosen as  $q_\ell(\star|\cdot)$  and  $q_\alpha(\star|\cdot)$  in (4.1) respectively, and the exponential schedule (4.4) is employed for randomly switching between SMMALA and AM steps. With the help of empirical tuning, the hyperparameters are set to  $\lambda = 0.01$ ,  $\gamma = 0.001$  in (2.13) and  $r = 10/n_m$  in (4.4).

Closed-form derivatives and the proposal covariance matrix  $\epsilon^2 G^{-1}(\boldsymbol{\theta})$  are used in the Bayesian logistic regression example. On the other hand, automatic differentiation and the SoftAbs metric ([4]) approximation of  $\epsilon^2 G^{-1}(\boldsymbol{\theta})$  are exploited in the three more complex examples related to the t-distribution and the planetary systems with one and two planets.

All associated numerics and visualizations for the four examples are available in Appendix A. Table 2 gathers the effective sample size, runtime, efficiency and speed-up summaries, as these arise after averaging across the ten simulated chains per sampler. The running mean, autocorrelation and trace of one specimen chain per sampler out of the ten simulated chains are visualized by Figures 2 and 3.

A package, called `MAMALASampler`, implements MAMALA using the Julia programming language. `MAMALASampler` is based on `Klara`, a package for MCMC inference written in Julia by one of the three authors. `Klara` has been named after Klara Dan von Neumann. `MAMALASampler` is open-source software available at

<https://github.com/scidom/MAMALASampler.jl>

along with the four examples of this paper. The `ForwardDiff` package, which is also written in Julia ([50]) and provides forward-mode automatic differentiation functionality, is put into practice in the simulations associated with the t-distribution and the planetary systems.

5.1. *Bayesian logistic regression.* As a first example, consider a Bayesian logistic regression model consisting of  $n_d$  samples and  $n_\theta$  covariates. The log-likelihood of the model expresses as

$$(5.1) \quad \mathcal{L}(\mathbf{y}, X|\boldsymbol{\theta}) = (X\boldsymbol{\theta})^T \mathbf{y} - \sum_{i=1}^{n_d} \log(1 + \exp(\boldsymbol{\theta}^T \mathbf{x}_i)),$$

where  $y \in \{0, 1\}^{n_d}$  is the binary response variable,  $X$  the  $n_d \cdot n_\theta$  design matrix,  $\mathbf{x}_i$  the  $i$ -th row of  $X$  and  $\boldsymbol{\theta} \in \mathbb{R}^{n_\theta}$  the regression coefficients. A normal prior is assumed for the model parameters  $\boldsymbol{\theta} \sim \pi(\boldsymbol{\theta}) = \mathcal{N}(\mathbf{0}, vI)$  for some positive hyperparameter  $v$ . The unnormalized log-target density for Bayesian logistic regression thus takes the form

$$(5.2) \quad \log(p(\boldsymbol{\theta}|\mathbf{y}, X)) = \mathcal{L}(\mathbf{y}, X|\boldsymbol{\theta}) + \log(\pi(\boldsymbol{\theta})),$$

where the log-likelihood is given by (5.1).

Differentiating (5.1) gives the gradient of the log-likelihood

$$(5.3) \quad \nabla_{\boldsymbol{\theta}}(L(\mathbf{y}, X|\boldsymbol{\theta})) = X^T \left( \mathbf{y} - \frac{1}{1 + \exp(-X\boldsymbol{\theta})} \right).$$

The gradient of the log-prior evaluates as

$$(5.4) \quad \nabla_{\boldsymbol{\theta}}(\log(\pi(\boldsymbol{\theta}))) = -\frac{1}{v}\boldsymbol{\theta}.$$

So, the gradient  $\nabla_{\boldsymbol{\theta}}(\log(p(\boldsymbol{\theta}|\mathbf{y}, X)))$  of the log-target equals the sum of (5.3) and (5.4).

The metric of a log-target  $\log(p)$  is conventionally taken to be the expected Fisher information of  $\log(p)$ , which is equal to the negative Hessian of log-likelihood  $L$  minus the Hessian of log-prior  $\log(\pi)$  in a Bayesian setting. By differentiating (5.3) and (5.4), it is deduced that the metric  $G(\boldsymbol{\theta}|X)$  for the Bayesian logistic regression model with a normal prior  $\mathcal{N}(\mathbf{0}, vI)$  is

$$(5.5) \quad G(\boldsymbol{\theta}|X) = X^T \Lambda(\boldsymbol{\theta}) X + \frac{1}{v} I,$$

where the  $n_d \cdot n_d$  diagonal matrix  $\Lambda(\boldsymbol{\theta}) = \text{diag}[p_i(1 - p_i)]$  has diagonal elements

$$(5.6) \quad p_i = P(y_i = 1) = \exp(\boldsymbol{\theta}^T \mathbf{x}_i) / (1 + \exp(\boldsymbol{\theta}^T \mathbf{x}_i)), \quad i \in \{1, 2, \dots, n_d\}.$$

Both the log-target gradient  $\nabla_{\boldsymbol{\theta}}(\log(p(\boldsymbol{\theta}|\mathbf{y}, X)))$  and metric  $G(\boldsymbol{\theta}|X)$  are needed for SMMALA proposals made by MAMALA.

MALA, AM, SMMALA and MAMALA are run on the bank dataset taken from [14] with the Bayesian logistic regression log-target outlined in the current section and with the prior hyperparameter set to  $v = 100$ , which implies a flat non-informative prior. The bank dataset contains the measurements of  $n_{\theta} = 4$  covariates on  $n_d = 200$  Swiss banknotes, 100 of which are genuine and 100 counterfeit. The four covariates include the bill length, the left and right edge width, and the bottom margin width. The binary response variable is the type of banknote, 0 being genuine and 1 counterfeit.

Table 2 shows the ESS for each of the four parameter coordinates  $\theta_i$ ,  $i \in \{1, 2, 3, 4\}$ . Figure 2b gives an idea of the autocorrelation for the second parameter coordinate  $\theta_2$ . According to Table 2 and Figure 2b, MAMALA has better mixing than AM and worse mixing than MALA and SMMALA for the current example of Bayesian logistic regression. Moreover, MAMALA exhibits shorter CPU runtime than AM and SMMALA, but longer runtime than MALA.

In terms of overall speed-up, MAMALA outperforms AM, but does worse than MALA and SMMALA. The relatively low computational complexity of log-target (5.2) and the presence of only  $n_{\theta} = 4$  parameters imply that linear algebra computations outweigh differentiation costs, thus explaining why MAMALA does not overtake MALA and SMMALA in this example.

5.2. *Multivariate t-distribution.* Monte Carlo samples are drawn from an  $n_{\theta}$ -dimensional Student- $t$  target  $t_{\nu}(\mathbf{0}, \frac{\nu-2}{\nu} \Sigma(c))$  with  $\nu$  degrees of freedom

and covariance matrix

$$(5.7) \quad \Sigma(c) = \begin{pmatrix} 1 & c^1 & c^2 & \dots & c^{n_\theta-3} & c^{n_\theta-2} & c^{n_\theta-1} \\ c^1 & 1 & c^1 & \dots & c^{n_\theta-4} & c^{n_\theta-3} & c^{n_\theta-2} \\ c^2 & c^1 & 1 & \dots & c^{n_\theta-5} & c^{n_\theta-4} & c^{n_\theta-3} \\ \vdots & \vdots & \vdots & \ddots & \vdots & \vdots & \vdots \\ c^{n_\theta-3} & c^{n_\theta-4} & c^{n_\theta-5} & \dots & 1 & c^1 & c^2 \\ c^{n_\theta-2} & c^{n_\theta-3} & c^{n_\theta-4} & \dots & c^1 & 1 & c^1 \\ c^{n_\theta-1} & c^{n_\theta-2} & c^{n_\theta-3} & \dots & c^2 & c^1 & 1 \end{pmatrix}$$

for some constant  $0 < c < 1$  that determines the level of correlation between parameter coordinates. The elements of the  $i$ -th diagonal of the  $n_\theta \cdot n_\theta$  covariance matrix  $\Sigma(c)$  equal  $c^{i-1}$ ,  $i = 1, 2, \dots, n_\theta$ . The scale matrix  $\frac{\nu-2}{\nu}\Sigma(c)$  of the  $t$ -distribution scales  $\Sigma(c)$  by a factor of  $\frac{\nu-2}{\nu}$  so that the covariance matrix of the  $t$ -distribution is  $\Sigma(c)$ .

In this example, the setting is not Bayesian, so there is no prior distribution involved ([48]). Instead, MCMC sampling acts as a random number generator to simulate from a  $t$ -distribution  $t_\nu(\mathbf{0}, \frac{\nu-2}{\nu}\Sigma(c))$ . The simulated chains are randomly initialized away from the zero mode of the  $t$ -distribution, and they are expected to converge to zero. In other words, the zero mode of  $t_\nu(\mathbf{0}, \frac{\nu-2}{\nu}\Sigma(c))$  is seen as the parameter vector to be estimated.

The dimension of the  $t$ -target is increased to  $n_\theta = 20$  from the  $n_\theta = 4$  parameters of the Bayesian logistic regression model, relatively high correlation is induced by selecting  $c = 0.9$  in (5.7), and some amount of probability mass is maintained in the  $t$ -distribution tails by choosing  $\nu = 30$  degrees of freedom. The present example does not reach the realm of a fully-fledged application, especially in terms of log-target complexity, yet it gives a first indication of some common computational costs appearing in more realistic applications, including automatic differentiation and SoftAbs metric evaluations.

Figure 2e displays the running means of four chains that correspond to the seventeenth coordinate  $\theta_{17}$  of the twenty-dimensional parameter vector  $\boldsymbol{\theta} \sim t_\nu(\mathbf{0}, \frac{28}{30}\Sigma(0.9))$ , with a single chain generated by each of MALA, AM, SMMALA and MAMALA. The running mean of the chain simulated using MALA does not appear to converge rapidly to the true mode of zero. This accords with theoretical knowledge. In particular, [55] and [39] have shown that if a target density has tails heavier than exponential or lighter than Gaussian, then a MALA proposal kernel does not yield a geometrically ergodic Markov chain. Furthermore, it can be seen that the chain generated by MAMALA converges faster than the chains produced by AM, MALA and SMMALA.

Table 2 reports the minimum, mean, median and maximum ESS of the  $n_\theta = 20$  parameter coordinates. As seen from Table 2, MAMALA achieves roughly ten times larger ESS in comparison to AM, MALA and SMMALA for the t-distribution example. Figures 2f, 3a, 3c, 3e and 3g show the autocorrelation and trace plots of the four chains with running means presented by Figure 2e. Figure 2f demonstrates that MAMALA has the lowest autocorrelation among the four compared samplers. The trace plots provide further circumstantial evidence of the faster mixing of MAMALA for the Student-t target. The mixing properties of MAMALA in the case of t-distribution come as a surprise, since MAMALA was designed to reduce the cost paid for faster mixing rather than to achieve the fastest possible mixing in absolute terms. MAMALA has shorter CPU runtime than SMMALA, but longer runtime than MALA and AM.

With a speed-up of 3.18, MAMALA is about three times more efficient than MALA and orders of magnitude more efficient than AM and SMMALA for the Student-t target  $t_\nu(\mathbf{0}, \frac{28}{30}\Sigma(0.9))$  of this second example.

5.3. *Radial velocity of a star in planetary systems.* The study of exoplanets has emerged as an important area of modern astronomy. While astronomers utilize a variety of different methods for detecting and characterizing the properties of exoplanets and their orbits, each of the prolific methods to date shares several characteristics. First, translating astronomical observations into planet physical and orbital properties requires significant statistical analysis. Second, characterizing planetary systems with multiple planets requires working with high-dimensional parameter spaces. Third, the posterior probability distributions are often complex with correlated parameters, non-linear correlations or multiple posterior modes. MCMC has proven invaluable for providing accurate estimates of planet properties and orbital parameters and is now used widely in the field.

For analyzing simple data sets such as one planet detected at high signal-to-noise ratio, random walk Metropolis-Hastings is effective and the choice of MCMC sampling algorithm is unlikely to be important ([16]). For analyzing more complex data sets such as a star with several planets, more care is necessary to avoid poor mixing of the Markov chains. One approach is “artisanal” MCMC, where proposal distributions are hand-crafted for a particular problem by making use of physical intuition and validation on simulated data sets ([15]). However, it is desirable to identify more sophisticated algorithms that can be efficient with minimal tuning or human intervention. Here, MAMALA is applied to simulated radial velocity planet search data sets so as to illustrate the potential of the sampler for future astronomical

or other scientific applications.

One of the most prolific methods for characterizing the orbits of extrasolar planets is the radial velocity method. Astronomers make a series of precise measurements of the line-of-sight velocity of a target star. The velocity of the star  $v(t)$  changes with time  $t$  due to the gravitational tug of any planets orbiting it. A basic radial velocity data set consists of a list of  $n_d$  observation times  $t_i$ ,  $i = 0, 1, \dots, n_d - 1$ , and measured velocities  $\hat{v}_i$ .

The observed velocity  $\hat{v}_i$  of the star at time  $t_i$  is modelled as the unknown velocity  $v(t_i)$  plus some measurement error  $\epsilon_i$ , as seen in (5.8). For many planetary systems with  $n_p$  planets, the stellar line-of-sight velocity  $v(t_i)$  can typically be well approximated by (5.9). Independent Gaussian measurement errors  $\epsilon_i$  with variances  $\sigma_i^2$  are assumed according to (5.10). Expressions (5.8), (5.9) and (5.10) introduce the following model for the radial velocity of a star in a planetary system consisting of  $n_p$  planets:

$$(5.8) \quad \hat{v}_i = v(t_i) + \epsilon_i,$$

$$(5.9) \quad v(t_i) = C + \sum_{j=1}^{n_p} K_j (\cos(\omega_j + T(t_i, P_j, e_j, M_{0,j})) + e_j \cos(\omega_j)),$$

$$(5.10) \quad \epsilon_i \sim \mathcal{N}(0, \sigma_i^2).$$

In (5.9),  $C$  is the systemic line-of-sight velocity of the planetary system,  $K_j$  is the velocity amplitude induced by the  $j$ -th planet,  $P_j$  is the orbital period of the  $j$ -th planet,  $e_j$  is the orbital eccentricity of the  $j$ -th planet,  $M_{0,j}$  is the mean anomaly at time  $t_0 = 0$  of the  $j$ -th planet,  $\omega_j$  is the argument of pericenter of the  $j$ -th planet, and  $T(t_i, P_j, e_j)$  is the true anomaly at time  $t_i$  of the  $j$ -th planet.

The true anomaly  $T$  is an angle that specifies the location of the planet and star along their orbit at a given time. The true anomaly  $T$  is related to the eccentric anomaly  $E$  by  $\tan(T/2) = \sqrt{\frac{1+e}{1-e}} \tan(E/2)$ . The eccentric anomaly  $E$  can be calculated from the mean anomaly  $M$  from Kepler's equation,  $M = E - E \sin(E)$ , and an iterative solver. The mean anomaly  $M$  increases at a linear rate with time and is given by  $M(t) = M_0 + 2\pi t/P$ .

It becomes apparent from (5.9) that a five-dimensional parameter vector  $\theta_j = (K_j, P_j, e_j, M_{0,j}, \omega_j)$  is associated with the  $j$ -th planet. Thus, a total of  $n_\theta = 5n_p + 1$  model parameters  $\theta = (C, \theta_1, \theta_2, \dots, \theta_{n_p})$  appear in a planetary system with  $n_p$  planets. The notation  $v(t_i, \theta)$  can be used in place of  $v(t_i)$  to indicate that the stellar line-of-sight velocity (5.9) of the star depends on the parameters  $\theta$ .

According to (5.10), the sum of squares of the normalized measurement

errors  $\epsilon_i/\sigma_i$  follow a chi-squared distribution with  $n_d$  degrees of freedom,

$$(5.11) \quad \sum_{i=0}^{n_d-1} \left( \frac{\epsilon_i}{\sigma_i} \right)^2 \sim \chi_{n_d}^2.$$

The log-likelihood arises from (5.11) and (5.8) as

$$(5.12) \quad \mathcal{L}(\mathbf{t}, \hat{\mathbf{v}}, \boldsymbol{\sigma} | \boldsymbol{\theta}) = -\frac{1}{2} \sum_{i=0}^{n_d-1} \left( \frac{v(t_i, \boldsymbol{\theta}) - \hat{v}_i}{\sigma_i} \right)^2,$$

where  $\mathbf{t} = (t_0, t_1, \dots, t_{n_d-1})$ ,  $\hat{\mathbf{v}} = (\hat{v}_0, \hat{v}_1, \dots, \hat{v}_{n_d-1})$ ,  $\boldsymbol{\sigma} = (\sigma_0, \sigma_1, \dots, \sigma_{n_d-1})$ . It is assumed that the measurement uncertainties  $\boldsymbol{\sigma}$  are known, so  $\mathbf{t}$ ,  $\hat{\mathbf{v}}$  and  $\boldsymbol{\sigma}$  make up the available data.

For the relatively simple model described by (5.12) and (5.9), astronomers commonly use a set of priors elicited during a 2013 SAMSI program on astrostatistics. Modified Jefferys priors are adopted for the velocity amplitudes  $K_j$  and orbital periods  $P_j$ . Uniform priors are employed for the orbital eccentricities  $e_j$ , velocity offsets  $M_{0,j}$  and angle offsets  $\omega_j$ , namely  $e_j \sim \text{Uniform}[0, 1)$ ,  $\omega_j \sim \text{Uniform}[0, 2\pi)$ ,  $M_{0,j} \sim \text{Uniform}[0, 2\pi)$ .

MAMALA is benchmarked on two simulated data sets, of which one consists of  $n_p = 1$  planet and the other one comprises  $n_p = 2$  planets. In each case,  $n_d = 50$  observed velocities  $\hat{\mathbf{v}} \in \mathbb{R}^{n_d}$  are simulated at times  $\mathbf{t} \in \mathbb{R}^{n_d}$  spread uniformly over two years.

**5.3.1. One-planet system.** For the one-planet system, the isochronal velocities  $\hat{v}_i$  are simulated using  $C = 1.0$ ,  $K_1 = 20m/s$ ,  $P_1 = 50$  days,  $e_1 = 0.2$ ,  $M_{0,1} = \pi/4$ ,  $\omega_1 = \pi/4$  and  $\sigma_i = 2m/s$  for  $i = 0, 1, \dots, 49$ . The parameter vector for this one-planet system is  $\boldsymbol{\theta} = (C, K_1, P_1, e_1, M_{0,1}, \omega_1)$ , so  $n_\theta = 6$  parameters are simulated from the target built upon log-likelihood (5.12).

Figure 2e shows the running means of four chains for the velocity amplitude  $K_1$  induced by the single planet, with one chain generated by each of the four compared samplers. SMMALA and MAMALA seem to converge to the same value, although the latter appears to converge faster.

Table 2 provides the minimum, mean, median and maximum ESS of the  $n_\theta = 6$  astronomical parameters  $\boldsymbol{\theta} = (C, K_1, P_1, e_1, M_{0,1}, \omega_1)$ . As seen from Table 2 and Figure 2f, MAMALA exhibits the largest ESS and smallest autocorrelation and therefore appears to have the fastest mixing. In terms of CPU runtime, MAMALA is about three times faster than SMMALA, but slower than MALA and AM.

Apart from attaining the fastest mixing, MAMALA outperforms MALA by a factor of 246.59 in terms of speed-up and SMMALA by a factor of even

higher order of magnitude. MAMALA has the second-best efficiency, with AM being the most efficient by reaching a 378.50 speed-up in comparison to MALA. The higher efficiency of AM over MAMALA for this example is attributed to the relatively small dimension  $n_\theta = 6$  of the parameter space. MAMALA might still be preferred over AM for this low-dimensional one-planet system, considering that the former sampler has higher ESS and higher acceptance rate than the latter at a relatively modest additional computational cost.

**5.3.2. Two-planet system.** For the two-planet system, the isochronal velocities  $\hat{v}_i$  are simulated using  $C = 1.0$ ,  $K_1 = K_2 = 30m/s$ ,  $P_1 = 40$  days,  $P_2 = 80.8$  days,  $e_1 = e_2 = 0.2$ ,  $M_{0,1} = M_{0,2} = \pi/4$ ,  $\omega_1 = \omega_2 = \pi/4$  and  $\sigma_i = 2m/s$  for  $i = 0, 1, \dots, 49$ . The parameter vector for this two-planet system is  $\theta = (C, K_1, P_1, e_1, M_{0,1}, \omega_1, K_2, P_2, e_2, M_{0,2}, \omega_2)$ , so  $n_\theta = 11$  parameters are simulated from the target built upon log-likelihood (5.12).

Figure 2g displays the running means of four chains for the velocity amplitude  $K_1$  induced by planet one of the two-planet system, with one chain generated by each of the four compared samplers. MAMALA seems to converge the fastest, followed by SMMALA. AM does not show signs of convergence, which is related to the low acceptance rate of AM in this example.

Table 2 provides the minimum, mean, median and maximum ESS of the  $n_\theta = 11$  parameters  $\theta = (C, K_1, P_1, e_1, M_{0,1}, \omega_1, K_2, P_2, e_2, M_{0,2}, \omega_2)$ . Similarly to the one-planet system, MAMALA attains the highest ESS, lowest autocorrelation and most rapidly mixing trace in the case of the two-planet system, as seen from Table 2 and Figures 2h, 3b, 3d, 3f and 3h.

The MALA trace plot of Figure 3b is characterized by slow exploration of the state space of parameter  $K_1$ , which is attributed to the small stepsize required for maintaining an acceptance rate close to the optimal rate of 57.4%. Although the AM chain of Figure 3d takes longer proposal steps than its MALA counterpart, AM suffers from a very low acceptance rate of 0.01%. SMMALA offers a substantial improvement in mixing over MALA and AM according to Figure 3f, while MAMALA appears to have the most rapid mixing among the four samplers (Figure 3h).

MAMALA ranks third in absolute runtime behind AM and MALA for the system of two planets (Table 2). However, AM does not work in the case of two planets, since it fails to converge and it has a prohibitively low acceptance rate of 0.01%. Besides, MALA does not seem to converge either and it explores the state space very slowly. In fact, the superiority of MAMALA in this example is depicted by the largest ESS and highest overall efficiency, with a relative speed-up about 25 and 20 times higher

than MALA and SMMALA, respectively.

5.4. *Synopsis of empirical results from simulations.* MAMALA has the highest ESS and thus the fastest mixing in three out of four examples, namely in the simulations from the t-distribution and from the two planetary systems. This empirical finding might indicate that some random transition kernels or combinations of transition kernels have better mixing properties than proposal mechanisms based on solitary geometric kernels.

In the two most computationally demanding out of the four examples (t-distribution and two-planet system), MAMALA manifested its capacity to achieve the highest speed-up among its competing samplers. Thus, combining kernels might help achieve high mixing per step with low computational cost per step for a range of models.

Simulation experimentation has led empirically to an optimal acceptance rate between 20% and 40% for MAMALA. This might be explained by the fact that AM contributes the majority of Monte Carlo steps to MAMALA for relatively small values of the tuning parameter  $r$  in (4.4).

**6. Discussion.** MCMC methods have proven critical to the adoption of Bayesian parameter estimation in many scientific and engineering disciplines. Despite advancements in computer hardware technologies, there will always be a tension between model complexity and computational resources. For many realistic applications, traditional MCMC methods struggle even in moderately-high dimensional parameter spaces, due to target densities with atypical local dependencies often induced by latent variables. Geometric MCMC methods hold considerable promise for improving the mixing properties of posterior sampling for such applications. However, existing manifold MCMC algorithms can rapidly become prohibitively expensive with increasing parameter dimensionality for problems with costly model evaluations. Therefore, developing geometric MCMC algorithms that are computationally feasible for such problems has the potential to enable inference for more realistic models.

This paper initiates a conceptually straightforward, yet potentially powerful, approach to the problem of making manifold MCMC algorithms more computationally accessible. The main idea is to combine geometric and non-geometric transition kernels to find a balance between computational cost and fast mixing. MAMALA has been empirically validated on simple statistical models and on slightly more complex astronomical models of planetary systems. These initial simulation studies reveal the potential of MAMALA in terms of performance relative to previous algorithms such as SMMALA. The increased effective sample size per model evaluation might have a bigger

impact for even more complex models with more model parameters or with more expensive target densities.

For example, astronomical models for the accurate characterization of the masses and orbits of extrasolar planets have high computational complexity. A target density defined by a typical planetary system with one star and  $n_p$  planets consists of at least  $5n_p + 1$  parameters and requires integrating a set of  $6n_p$  first-order ordinary differential equations. Ensemble samplers, such as the differential evolution MCMC ([5, 45]) and the affine-invariant sampler ([20, 31, 41]), have been adapted by the astrophysics community to perform Bayesian inference on planetary systems given exoplanet observations. Even if the differential evolution MCMC algorithm is parallelized over a cluster of CPUs or a GPU, acquiring posterior samples for such systems requires weeks of computation ([12, 9, 47, 32, 43]).

For some planetary systems, the mutual gravitational interactions can be ignored, so using a simpler approximate model to emulate a more expensive model can dramatically reduce the computational cost. However, many of the most scientifically interesting planetary systems and data sets require using the full and more expensive model, including Doppler observations of near-resonant planetary systems and transit timing measurements for near-resonant or tightly packed systems.

MCMC algorithms that exploit geometric information about the posterior shape are likely to be more efficient in terms of the absolute number of model evaluations. Manifold MCMC methods could make it practical to generate posterior samples with increased effective sample sizes. Unfortunately, computing partial derivatives for every proposal, as required for MMALA or SMMALA, would be extremely expensive. MAMALA algorithms have the potential to significantly reduce the number of gradient and Hessian evaluations required, and are thus expected to accelerate computations by over an order of magnitude relative to SMMALA for expensive models.

Costly models, such as systems of differential equations, often give rise to multi-modal target densities representing intricate dependencies among parameters. Sampling methods may be embedded in a population MCMC framework to allow better exploration of and convergence to challenging targets ([19]). Along these lines, future research may use MAMALA in place of SMMALA within a population MCMC scheme to perform inference on expensive models involving systems of differential equations.

MAMALA opens up possible avenues of methodological research for building proposal mechanisms based on random transition kernels or on transition kernel combinations. Exploring ways of injecting local geometric information in alternative adaptive or other non-geometric MCMC methods promises to

make manifold MCMC more amenable to realistic applications.

## APPENDIX A: DESCRIPTIVE STATISTICS OF SIMULATION STUDY

The appendix is made up of Table 2 and Figures 2 and 3, which provide numerical and visual summaries associated with the simulation study of section 5.

## ACKNOWLEDGEMENTS

This paper was supported by the National Aeronautics and Space Administration (NASA) under grant NNX15AE21G issued through the Exoplanet Research Program. E.B.F. acknowledges the support of the Eberly College of Science, Center for Astrostatistics, Institute for CyberScience and Center for Exoplanets and Habitable Worlds of Pennsylvania State University, USA. The Center for Exoplanets and Habitable Worlds is supported by the Pennsylvania State University, the Eberly College of Science, and the Pennsylvania Space Grant Consortium. The results reported herein benefited from collaborations and/or information exchange within the Nexus for Exoplanet System Science (NExSS) research coordination network sponsored by the Science Mission Directorate (SMD) of NASA.

## REFERENCES

- [1] AARTS, E. and KORST, J. (1989). *Simulated annealing and Boltzmann machines: a stochastic approach to combinatorial optimization and neural computing*. John Wiley & Sons, Inc.
- [2] ANDRIEU, C. and MOULINES, E. (2006). On the ergodicity properties of some adaptive MCMC algorithms. *Ann. Appl. Probab.* **16**: 1462–1505. [MR2260070](#)
- [3] BAI, Y. and ROBERTS, G. O. and ROSENTHAL, J. S. (2011). On the containment condition for adaptive Markov chain Monte Carlo algorithms. *Adv. Appl. Stat.* **21**: 1–54. [MR2849670](#)
- [4] BETANCOURT, M. (2013). A general metric for Riemannian manifold Hamiltonian Monte Carlo. *Geometric Science of Information: First International Conference*. 327–334. [MR3126061](#)
- [5] BRAAK, C. J. F. T. (2006). A Markov chain Monte Carlo version of the genetic algorithm differential evolution: easy Bayesian computing for real parameter spaces. *Stat. Comput.* **16**: 239–249. [MR2242236](#)
- [6] BYRNE, S. and GIROLAMI, M. (2013). Geodesic Monte Carlo on embedded manifolds. *Scand. J. Stat.* **40**: 825–845.
- [7] CALDERHEAD, B. and EPSTEIN, M. and SIVILOTTI, L. and GIROLAMI, M. (2013). Bayesian approaches for mechanistic ion channel modeling. *Methods Mol. Biol.* **1021**: 247–272.
- [8] CALDERHEAD, B. and GIROLAMI, M. (2011). Statistical analysis of nonlinear dynamical systems using differential geometric sampling methods. *Interface Focus*. 821–835.
- [9] CARTER, J. A. and AGOL, E. and CHAPLIN, W. J. and BASU, S. and BEDDING, T. R. and BUCHHAVE, L. A. and CHRISTENSEN-DALSGAARD, J. and DECK, K. M. and

- ELSWORTH, Y. and FABRYCKY, D. C. and FORD, E. B. and FORTNEY, J. J. and HALE, S. J. and HANDBERG, R. and HEKKER, S. and HOLMAN, M. J. and HUBER, D. and KAROFF, C. and KAWALER, S. D. and KJELDSSEN, H. and LISSAUER, J. J. and LOPEZ, E. D. and LUND, M. N. and LUNDKVIST, M. and METCALFE, T. S. and MIGLIO, A. and ROGERS, L. A. and STELLO, D. and BORUCKI, W. J. and BRYSON, S. and CHRISTIANSEN, J. L. and COCHRAN, W. D. and GEARY, J. C. and GILLILAND, R. L. and HAAS, M. R. and HALL, J. and HOWARD, A. W. and JENKINS, J. M. and KLAUS, T. and KOCH, D. G. and LATHAM, D. W. and MACQUEEN, P. J. and SASSELOV, D. and STEFFEN, J. H. and TWICKEN, J. D. and WINN, J. N. (2012). Kepler-36: A pair of planets with neighboring orbits and dissimilar densities. *Science*. **337**: 556–559.
- [10] CHIB, S. and GREENBERG, E. (1995). Understanding the Metropolis-Hastings algorithm. *Amer. Statist.* **49**: 327–335.
- [11] DAVIE, A. M. and STOTHERS, A. J. (2013). Improved bound for complexity of matrix multiplication. *Proc. Roy. Soc. Edinburgh Sect. A*. **143**: 351–369. [MR3039815](#)
- [12] DOYLE, L. R. and CARTER, J. A. and FABRYCKY, D. C. and SLAWSON, R. W. and HOWELL, S. B. and WINN, J. N. and OROSZ, J. A. and PRŠA, A. and WELSH, W. F. and QUINN, S. N. and LATHAM, D. and TORRES, G. and BUCHHAVE, L. A. and MARCY, G. W. and FORTNEY, J. J. and SHPORER, A. and FORD, E. B. and LISSAUER, J. J. and RAGOZZINE, D. and RUCKER, M. and BATALHA, N. and JENKINS, J. M. and BORUCKI, W. J. and KOCH, D. and MIDDOUR, C. K. and HALL, J. R. and MCCAULIFF, S. and FANELLI, M. N. and QUINTANA, E. V. and HOLMAN, M. J. and CALDWELL, D. A. and STILL, M. and STEFANIK, R. P. and BROWN, W. R. and ESQUERDO, G. A. and TANG, S. and FURESZ, G. and GEARY, J. C. and BERLIND, P. and CALKINS, M. L. and SHORT, D. R. and STEFFEN, J. H. and SASSELOV, D. and DUNHAM, E. W. and COCHRAN, W. D. and BOSS, A. and HAAS, M. R. and BUZASI, D. and FISCHER, D. (2011). Kepler-16: A transiting circumbinary planet. *Science*. **333**: 1602–1606.
- [13] DUANE, S. and KENNEDY, A. D. and PENDLETON, B. J. and ROWETH, D. (1987). Hybrid Monte Carlo. *Phys. Lett. B*. **195**: 216–222.
- [14] FLURY, B. and RIEDWYL, H. (1988). *Multivariate statistics*. Chapman and Hall.
- [15] FORD, E. B. (2006). Improving the efficiency of Markov chain Monte Carlo for analyzing the orbits of extrasolar planets. *Astrophys. J.* **642**: 505–522.
- [16] FORD, E. B. (2005). Quantifying the uncertainty in the orbits of extrasolar planets. *Astron. J.* **129**: 1706–1717.
- [17] GEYER, C. J. (1992). Practical Markov chain Monte Carlo. *Statist. Sci.* **7**: 473–483.
- [18] GILL, P. E. and GOLUB, G. H. and MURRAY, W. and SAUNDERS, M. A. (1974). Methods for modifying matrix factorizations. *Math. Comp.* **28**: 505–535. [MR0343558](#)
- [19] GIROLAMI, M. and CALDERHEAD, B. (2011). Riemann Manifold Langevin and Hamiltonian Monte Carlo Methods. *J. R. Stat. Soc. Ser. B. Stat. Methodol.* **73**: 123–214. [MR2814492](#)
- [20] GOODMAN, J. and WEARE, J. (2010). Ensemble samplers with affine invariance. *Commun. Appl. Math. Comput. Sci.* **5**: 65–80. [MR2600822](#)
- [21] GRIEWANK, A. (2014). On automatic differentiation and algorithm linearization. *Pesquisa Operacional*. **34**: 621–645.
- [22] GRIEWANK, A. and WALTHER, A. (2008). *Evaluating derivatives: principles and techniques of algorithmic differentiation*. SIAM.
- [23] GRIFFIN, J. E. and WALKER, S. G. (2013). On adaptive Metropolis-Hastings methods. *Stat. Comput.* **23**: 123–134. [MR3018354](#)
- [24] HAARIO, H. and LAINE, M. and MIRA, A. and SAKSMAN, E. (2006). DRAM: efficient

- adaptive MCMC. *Stat. Comput.* **16**: 339–354. [MR2297535](#)
- [25] HAARIO, H. and Saksman, E. and Tamminen, J. (2001). An adaptive Metropolis algorithm. *Bernoulli*. **7**: 223–242.
- [26] HAJEK, B. (1988). Cooling schedules for optimal annealing. *Math. Oper. Res.* **13**: 311–329. [MR0942621](#)
- [27] HIGHAM, N. J. (1988). Computing a nearest symmetric positive semidefinite matrix. *Linear Algebra Appl.* **103**: 103–118. [MR0943997](#)
- [28] HIGHAM, N. J. (2002). Computing the nearest correlation matrix - a problem from finance. *IMA J. Numer. Anal.* **22**: 329–343.
- [29] HIGHAM, N. J. and STRABIĆ, N. (2016). Anderson acceleration of the alternating projections method for computing the nearest correlation matrix. *Numer. Algorithms*. **72**: 1021–1042. [MR3529831](#)
- [30] HOUSE, T. (2015). Hessian corrections to the Metropolis adjusted Langevin algorithm. *arXiv*.
- [31] HOU, F. and GOODMAN, J. and HOGG, D. W. and WEARE, J. and SCHWAB, C. (2012). An affine-invariant sampler for exoplanet fitting and discovery in radial velocity data. *Astrophys. J.* **745**: 1–10.
- [32] JONTOF-HUTTER, D. and ROWE, J. F. and LISSAUER, J. J. and FABRYCKY, D. C. and FORD, E. B. (2015). The mass of the Mars-sized exoplanet Kepler-138 b from transit timing. *Nature*. **522**: 321–323.
- [33] KIRKPATRICK, S. and GELATT, C. D. and VECCHI, M. P. (1983). Optimization by simulated annealing. *Science*. **220**: 671–680.
- [34] KLEPPE, T. S. (2016). Adaptive step size selection for Hessian-based manifold Langevin samplers. *Scand. J. Stat.* **43**: 788–805. [MR3543323](#)
- [35] LAN, S. and STATHOPOULOS, V. and SHAHBABA, B. and GIROLAMI, M. (2015). Markov chain Monte Carlo from Lagrangian dynamics. *J. Comput. Graph. Statist.* **24**: 357–378. [MR3357385](#)
- [36] LAN, S. and STREETS, J. and SHAHBABA, B. (2014). Wormhole Hamiltonian Monte Carlo. *Proceedings of the 28th AAAI Conference on Artificial Intelligence*. 1953–1959.
- [37] LAN, S. and BUI, T. T. and CHRISTIE, M. and GIROLAMI, M. (2016). Emulation of higher-order tensors in manifold Monte Carlo methods for Bayesian inverse problems. *J. Comput. Phys.* **308**: 81–101. [MR3448239](#)
- [38] LE GALL, F. (2014). Powers of tensors and fast matrix multiplication. *ISSAC 2014 Proceedings of the 39th International Symposium on Symbolic and Algebraic Computation*. 296–303. [MR3239939](#)
- [39] LIVINGSTONE, S. and GIROLAMI, M. (2014). Information-geometric Markov chain Monte Carlo methods using diffusions. *Entropy*. **16**: 3074–3102. [MR3234224](#)
- [40] LOCATELLI, M. (2000). Simulated annealing algorithms for continuous global optimization: convergence conditions. *J. Optim. Theory Appl.* **104**: 121–133.
- [41] MACKEY, D. F. and HOGG, D. W. and LANG, D. and GOODMAN, J. (2013). emcee: the MCMC hammer. *Publ. Astron. Soc. Pac.* **125**: 306–312.
- [42] FERNANDO DIAZ MARTIN, J. and RIAÑO SIERRA, J. M. (2009). A comparison of cooling schedules for simulated annealing. *Encyclopedia of Artificial Intelligence*. 344–352.
- [43] MILLS, S. M. and FABRYCKY, D. C. and MIGASZEWSKI, C. and FORD, E. B. and PETIGURA, E. and ISAACSON, H. (2016). A resonant chain of four transiting, sub-neptune planets. *Nature*. **533**: 509–512.
- [44] NEAL, R. M. (1996). *Bayesian learning for neural networks*. Springer.
- [45] NELSON, B. and FORD, E. B. and PAYNE, M. J. (2014). RUN DMC: an Efficient, parallel code for analyzing radial velocity observations using n-body integrations and

- differential evolution Markov chain Monte Carlo. *Astrophys. J. Suppl. Ser.* **210**: 1–13.
- [46] NOURANI, Y. and ANDRESEN, B. (1998). A comparison of simulated annealing cooling strategies. *J. Phys. A: Math. Gen.* **31**: 8373–8385.
- [47] OROSZ, J. A. and WELSH, W. F. and CARTER, J. A. and FABRYCKY, D. C. and COCHRAN, W. D. and ENDL, M. and FORD, E. B. and HAGHIGHIPOUR, N. and MACQUEEN, P. J. and MAZEH, T. and SANCHIS-OJEDA, R. and SHORT, D. R. and TORRES, G. and AGOL, E. and BUCHHAVE, L. A. and DOYLE, L. R. and ISAACSON, H. and LISSAUER, J. J. and MARCY, G. W. and SHPORER, A. and WINDMILLER, G. and BARCLAY, T. and BOSS, A. P. and CLARKE, B. D. and FORTNEY, J. and GEARY, J. C. and HOLMAN, M. J. and HUBER, D. and JENKINS, J. M. and KINEMUCHI, K. and KRUSE, E. and RAGOZZINE, D. and SASSELOV, D. and STILL, M. and TENENBAUM, P. and UDDIN, K. and WINN, J. N. and KOCH, D. G. and BORUCKI, W. J. (2012). Kepler-47: a transiting circumbinary multiplanet system. *Science*. **337**: 1511–1514.
- [48] PAPAMARKOU, T. and Mira, A. and Girolami, M. (2015). Monte Carlo methods and zero variance principle. *Chapman and Hall/CRC*. 457–476.
- [49] PEREYRA, M. (2016). Proximal Markov chain Monte Carlo algorithms. *Stat. Comput.* **26**: 745–760. [MR3515019](#)
- [50] REVELS, J. and LUBIN, M. and PAPAMARKOU, T. (2016). Forward-mode automatic differentiation in Julia. *arXiv*.
- [51] ROBERTS, G. O. and ROSENTHAL, J. S. (2007). Coupling and ergodicity of adaptive Markov chain Monte Carlo algorithms. *J. Appl. Probab.* **44**: 458–475. [MR2340211](#)
- [52] ROBERTS, G. O. and ROSENTHAL, J. S. (2009). Examples of adaptive MCMC. *J. Comput. Graph. Statist.* **18**: 349–367. [MR2749836](#)
- [53] ROBERTS, G. O. and ROSENTHAL, J. S. (1998). Optimal scaling of discrete approximations to Langevin diffusions. *J. R. Stat. Soc. Ser. B. Stat. Methodol.* **60**: 255–268. [MR1625691](#)
- [54] ROBERTS, G. O. and STRAMER, O. (2002). Langevin diffusions and Metropolis-Hastings algorithms. *Methodol. Comput. Appl. Probab.* **4**: 337–357.
- [55] ROBERTS, G. O. and TWEEDIE, R. L. (1996). Exponential convergence of Langevin distributions and their discrete approximations. *Bernoulli*. **2**: 341–363. [MR1440273](#)
- [56] SAKSMAN, E. and VIHOLA, M. (2010). On the ergodicity of the adaptive Metropolis algorithm on unbounded domains. *Ann. Appl. Probab.* **20**: 2178–2203. [MR2759732](#)
- [57] SCHWENTNER, R. and PAPAMARKOU, T. and KAUER, M. O. and STATHOPOULOS, V. and YANG, F. and BILKE, S. and MELTZER, P. S. and GIROLAMI, M. and KOVAR, H. (2015). EWS-FLI1 employs an E2F switch to drive target gene expression. *Nucleic Acids Res.* **43**: 2780–2789.
- [58] SEEGER, M. (2004). Low rank updates for the Cholesky decomposition.
- [59] ŞİMŞEKLI, U. and BADEAU, R. and CEMGIL, A. T. and RICHARD, G. (2016). Stochastic quasi-Newton Langevin Monte Carlo. *International Conference on Machine Learning (ICML)*.
- [60] VIHOLA, M. (2012). Robust adaptive Metropolis algorithm with coerced acceptance rate. *Stat. Comput.* **22**: 997–1008 [MR2950080](#)
- [61] WILLIAMS, V. V. (2011). Breaking the Coppersmith-Winograd barrier.
- [62] WILKINSON, J. H. (1971). Modern error analysis. *SIAM Rev.* **13**: 548–568. [MR0305578](#)
- [63] XIFARA, T. and SHERLOCK, C. and LIVINGSTONE, S. and BYRNE, S. and GIROLAMI, M. (2014). Langevin diffusions and the Metropolis-adjusted Langevin algorithm. *Statist. Probab. Lett.* **91**, 14–19. [MR3208109](#)

T. PAPAMARKOU  
SCHOOL OF MATHEMATICS AND STATISTICS  
UNIVERSITY OF GLASGOW  
UNIVERSITY PLACE  
GLASGOW, G12 8SQ, UK  
E-MAIL: [theodore.papamarkou@glasgow.ac.uk](mailto:theodore.papamarkou@glasgow.ac.uk)

E. B. FORD  
CENTER FOR ASTROSTATISTICS  
INSTITUTE FOR CYBERSCIENCE  
CENTER FOR EXOPLANETS &  
HABITABLE WORLDS  
DEPARTMENT OF ASTRONOMY & ASTROPHYSICS  
525 DAVEY LAB  
THE PENNSYLVANIA STATE UNIVERSITY  
UNIVERSITY PARK, PA 16802, USA  
E-MAIL: [ebf11@psu.edu](mailto:ebf11@psu.edu)

A. LINDO  
SCHOOL OF MATHEMATICS AND STATISTICS  
UNIVERSITY OF GLASGOW  
UNIVERSITY PLACE  
GLASGOW, G12 8SQ, UK  
E-MAIL: [alexey.lindo@glasgow.ac.uk](mailto:alexey.lindo@glasgow.ac.uk)

TABLE 2

Comparison of sampling efficacy between MALA, AM, SMMALA and MAMALA for logistic regression,  $t$ -distribution, one-planet and two-planet system. AR: acceptance rate; ESS: effective sample size;  $t$ : CPU runtime in seconds; ESS/ $t$ : smaller ESS across model parameters divided by runtime; Speed: ratio of ESS/ $t$  for MALA over ESS/ $t$  for each other sampler. All tabulated numbers have been rounded to the second decimal place, apart from effective sample sizes, which have been rounded to the nearest integer. For logistic regression on the Swiss banknotes data, the ESS of each of four parameters  $\theta_i$ ,  $i \in \{1, 2, 3, 4\}$ , is provided. For the  $t$ -distribution, one-planet and two-planet system, the minimum, mean, median and maximum ESS across the effective sample sizes of the respective twenty, six and eleven parameters are displayed.

Logistic regression								
Method	AR	ESS				t	ESS/t	Speed
		$\theta_1$	$\theta_2$	$\theta_3$	$\theta_4$			
MALA	0.57	<b>23142</b>	8135	8804	8636	4.39	1851.70	<b>1.00</b>
AM	0.32	6475	6942	6654	6121	12.76	479.54	0.26
SMMALA	0.71	14515	<b>14189</b>	<b>13897</b>	<b>12118</b>	13.23	916.17	0.49
MAMALA	0.29	7308	7457	7251	6746	9.20	733.36	0.40
Student's $t$ -distribution								
Method	AR	ESS				t	ESS/t	Speed
		min	mean	median	max			
MALA	0.59	135	159	145	234	9.33	14.52	1.00
AM	0.03	85	118	117	155	17.01	5.03	0.35
SMMALA	0.71	74	87	86	96	143.63	0.52	0.04
MAMALA	0.26	<b>1471</b>	<b>1558</b>	<b>1560</b>	<b>1629</b>	31.81	46.23	<b>3.18</b>
One-planet system								
Method	AR	ESS				t	ESS/t	Speed
		min	mean	median	max			
MALA	0.55	4	76	18	394	57.03	0.07	1.00
AM	0.08	1230	1397	1279	2035	48.84	25.18	<b>378.50</b>
SMMALA	0.71	464	597	646	658	208.46	2.23	33.45
MAMALA	0.30	<b>1260</b>	<b>2113</b>	<b>2151</b>	<b>3032</b>	76.80	16.41	246.59
Two-planet system								
Method	AR	ESS				t	ESS/t	Speed
		min	mean	median	max			
MALA	0.59	5	52	10	377	219.31	0.02	1.00
AM	0.01	18	84	82	248	81.24	0.22	9.05
SMMALA	0.70	53	104	100	161	1606.92	0.03	1.37
MAMALA	0.32	<b>210</b>	<b>561</b>	<b>486</b>	<b>1110</b>	328.08	0.64	<b>26.39</b>

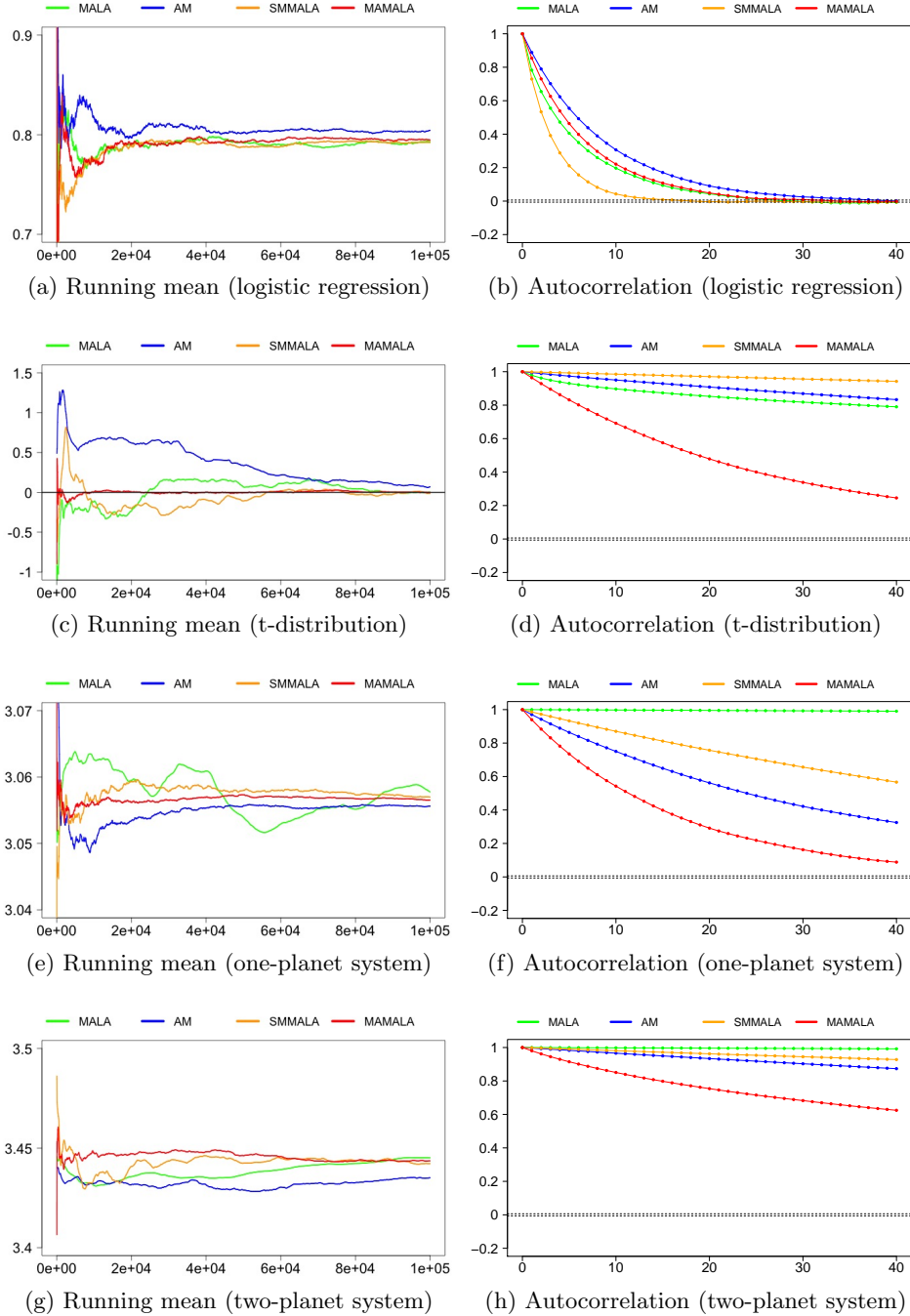
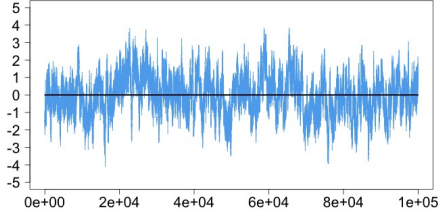
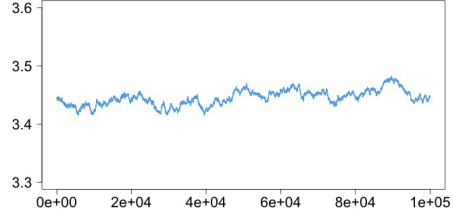


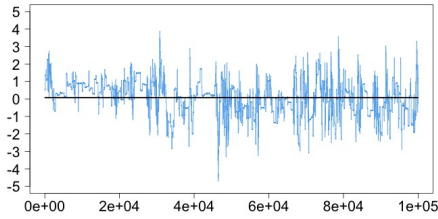
FIG 2. Overlaid running means and overlaid linear autocorrelations of single chains corresponding to one of the four, twenty, six and eleven parameters of the respective logistic regression,  $t$ -distribution, one-planet and two-planet system. The black horizontal line in the  $t$ -distribution running mean plot represents the true mode.



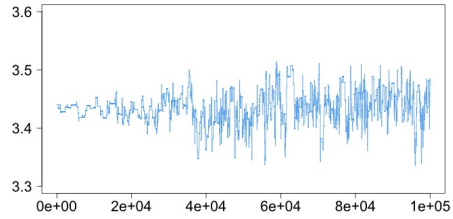
(a) MALA traceplot (t-distribution)



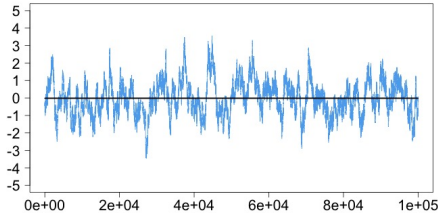
(b) MALA traceplot (two-planet system)



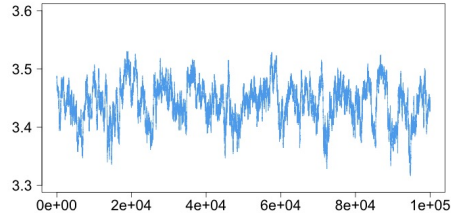
(c) AM traceplot (t-distribution)



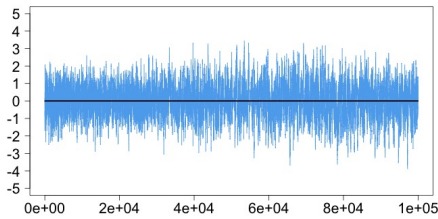
(d) AM traceplot (two-planet system)



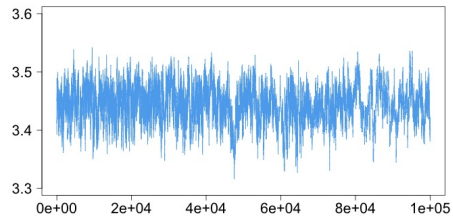
(e) SMMALA traceplot (t-distribution)



(f) SMMALA traceplot (two-planet system)



(g) MAMALA traceplot (t-distribution)



(h) MAMALA traceplot (two-planet system)

FIG 3. Trace plots of single chains corresponding to one of the twenty and eleven parameters of the respective  $t$ -distribution and two-planet system. The same chains were used for generating the trace plots of Figure 3 and the associated running means and autocorrelations of Figure 2. The black horizontal lines in the  $t$ -distribution trace plots represent the true mode.